SPIN AND PARITY ASSIGNMENT IN ^{152}Gd INVESTIGATING OCTUPOLE STRUCTURES

Suzan Phumudzo Bvumbi

Thesis presented in fulfillment of the requirements for the degree of Master of Sciences at the University of the Western Cape

Supervisor: Dr. D.G. Roux

Dept. of Physics

University of the Western Cape

Co-supervisors: Dr. S.M. Mullins

iThemba LABS

Prof. J.F. Sharpey-Schafer

Dept. of Physics

University of the Western Cape

December 2008

DECLARATION

I, the undersigned, hereby declare that the work contained in this thesis is my own original work and that I have not previously in its entirety or in part submitted it at any university for a degree.

Signature: ....

Date: ....

ABSTRACT

The high-spin states of the nucleus ^{152}Gd have been populated via the ^{152}Sm (α, 4n) ^{152}Gd fusion-evaporation reaction at a beam energy of 45MeV. The emitted γ rays were observed with the AFRODITE spectrometer array. The previously known decay scheme of ^{152}Gd was extended. Directional Correlation from Oriented states of nuclei (DCO) and linear polarization measurements were performed in order to assign spins and parities in the ^{152}Gd decay scheme. An alternative interpretation of the first excited $K^{\pi} = 0^{+}$ band, previously considered to be a β-vibration is discussed.

ACKNOWLEDGEMENTS

CONTENTS

LIST OF FIGURES

My role in this project was to analyze the ^{152}Gd data and to assign spin and parity to the energy levels in the deduced decay scheme. For this purpose, the multipolarity of the new γ-ray transitions had to be assigned. The techniques used will be the Directional Correlations of gamma rays from Oriented states of nuclei (DCO) and linear polarization of gamma rays. Our (α, 4n) data allowed us to extend the previously known decay scheme of ^{152}Gd.

The techniques used to assign spin and parity in the ^{152}Gd decay scheme will be discussed later in Chapter 2. The heavy-ion fusion reactions used to populate ^{152}Gd will also be discussed in Chapter 2. Relevant nuclear theory including ways in which gamma rays interact with the crystals of detectors and the correlations of gamma transitions will be discussed in Chapter 2. Chapter 3 gives brief description of the AFRODITE germanium array and the electronics, and details of the experiment. The data analysis and results obtained will be discussed in Chapter 4. Chapter 5 covers the spin and parity discussions for various bands in the ^{152}Gd decay scheme and their interpretations. The interpretation of bands section in Chapter 5 also covers the comparison of ^{152}Gd and the isotone ^{154}Dy.The conclusions reached and future experiments will be summarized in Chapter 6.
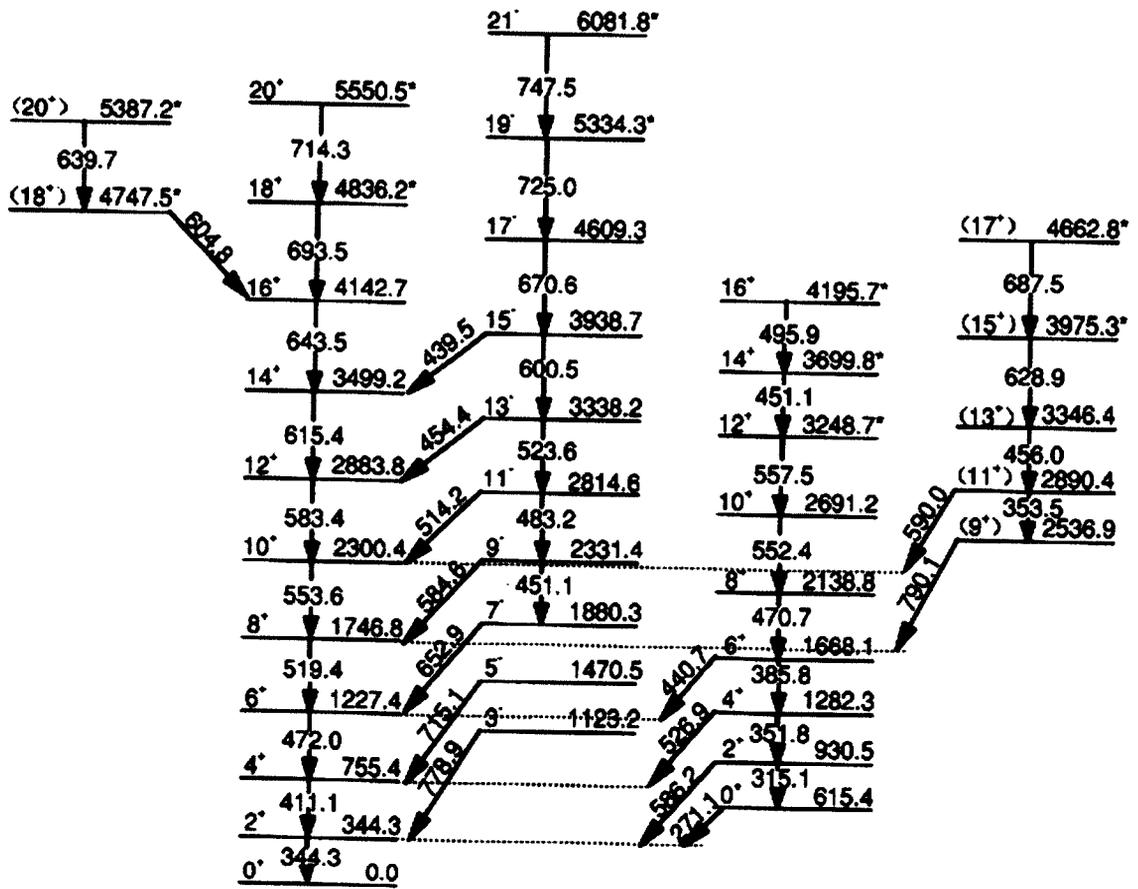
Figure 1.1: Decay scheme observed by [Wa05] from the (⁶Be, 5n) data.

CHAPTER 2 NUCLEAR THEORY

This thesis describes how spin and parity are assigned to excited states in atomic nuclei. Before the experimental techniques used to make these assignments are described, a brief summary will be given on the theory of collective excited states in nuclei. The different ways in which gamma photons can interact with matter will also be described. These are important because unless the γ-rays emitted from the nucleus can be measured in some sort of detector, it would not be possible to study nuclear structure. Heavy-ion fusion-evaporation reactions, and the techniques used (angular distribution, angular correlation, DCO and linear polarization) are also discussed in this chapter.

2.1 Nuclear shapes

Nuclei near closed shells are spherical. Outside closed shells they can deform and give surfaces that are usually given by an expansion in spherical harmonics Y_l^m, given by:

$$R(\theta, \varphi) = R_0 [1 + \sum_{l,m} \alpha_{lm} Y_{lm}(\theta, \varphi)] \qquad (2.1),$$

where m ranges from $-l$ to $+l$. $Y_{lm}(\theta, \varphi)$ are the spherical harmonics, and R_0 is the radius of a sphere which would have the same volume as the nucleus. By writing $\alpha_{20} = \beta \cos \gamma$ and $\alpha_{22} = \alpha_{2-2} = \beta \sin \gamma$ the nuclear shape can be specified in terms of β and γ. When $R(\theta, \varphi) = R_0$ the nucleus has a spherical shape, $\beta > 0$ and $\gamma = 0°$ gives an axially symmetric prolate nucleus (like a rugby ball) and $\beta < 0$ and $\gamma = 60°$ gives an axially symmetric oblate nucleus (like a pancake bun). The prolate or oblate shape refers to the orbital shape of a specific intrinsic configuration, which can be understood in terms of Nilsson diagrams. Most nuclei away from closed shells have permanent prolate quadrupole deformation. This means that the only spherical

2.2.1 Rotational bands

When a deformed nucleus in a particular intrinsic state rotates about an axis that is perpendicular to the symmetry axis, it generates discrete states of angular momentum of monotonically increasing energy and spin, and that are called rotational bands. There are different types of rotational bands, namely ground-state band of an even-even nucleus, strongly coupled band, and decoupled band. The ground state of an even-even nucleus (even-Z, even-N) is always a 0^+ state, and the rotational states in this case are restricted to even values of I. The ground state level is characterized by $I^\pi = 0^+$ because all the nucleons are coupled in spin-zero pairs, and summing all these pairs gives a total angular momentum of zero. The excited states in the rotational band are $I^\pi = 2^+, 4^+, 6^+, ...$ The excited states can be defined in terms of the nuclear wave function, given by:

$$\Psi_{IM} = \left(\frac{2I+1}{16\pi^2}\right)\left[D_{IMK}\chi_K + (-1)^{I-K}D_{IM-K}\chi_K\right] \tag{2.3},$$

Where D is the rotational wave function and χ is the intrinsic wave function. In the case of $K = 0$, Ψ_{IM} vanishes for odd I.

2.3 Heavy ion fusion evaporation reaction

Heavy ion fusion evaporation reactions are the best tool for the transfer of large amounts of angular momentum to the target nucleus. This reaction occurs when a projectile beam carrying an orbital angular momentum of $\vec{L} = \vec{r} \times \vec{p}$ is incident on a target nucleus, fusing with the target nucleus creating a compound nucleus that is highly excited with very high angular momentum. This excited nucleus then decays to its ground state via several processes; it could emit alpha particles, protons or neutrons, as shown in Fig. 2.2. These reactions produce nuclei with spins aligned in a plane perpendicular to the beam direction (oriented states).

The probability of emitting any of these depends on how deficient it is in any of these. When there is insufficient energy to emit charged particles or neutrons, the nucleus will lose angular momentum by emitting gamma rays all the way down to the ground state. The yrast states are states of lowest energy for a given total spin. After neutron evaporation is no longer possible, gamma rays are emitted and the de-excitation path closely tracks the yrast line, as shown in Fig. 2.3.
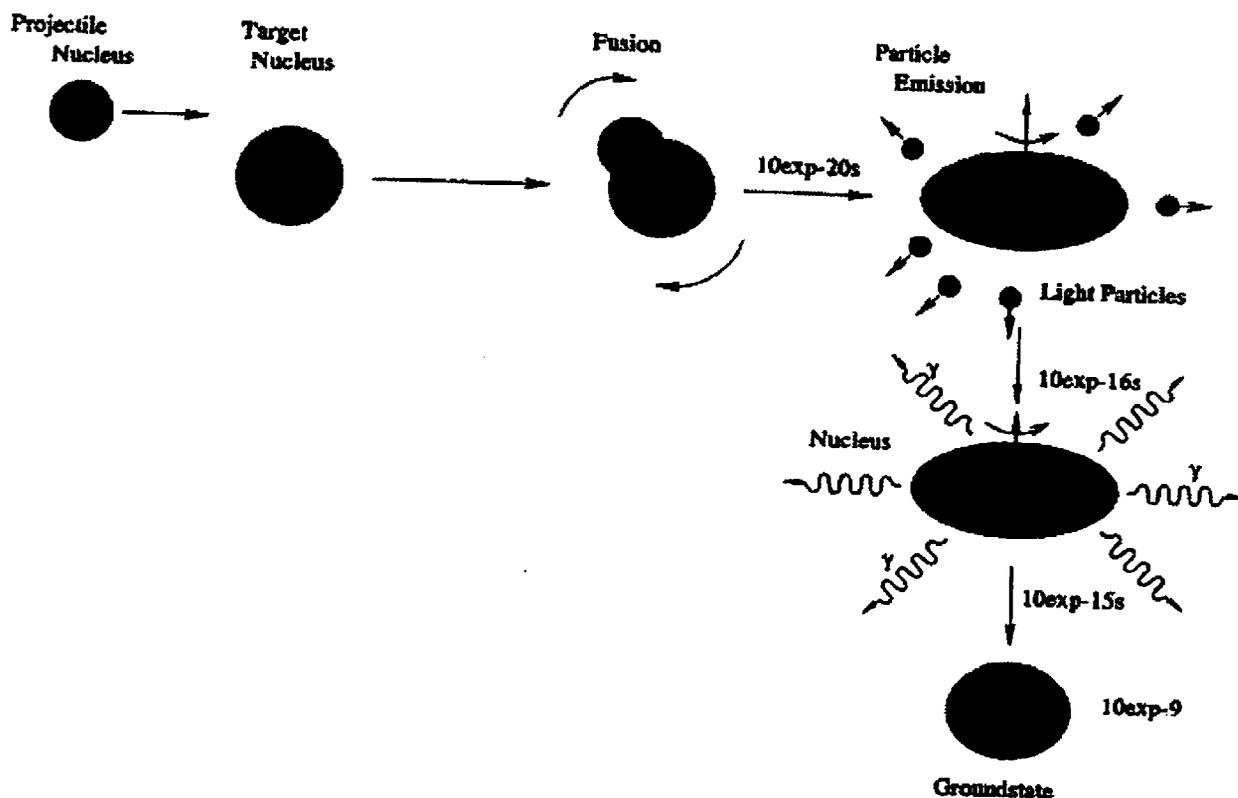
Figure 2.2: Formation of a compound nucleus in a heavy-ion fusion evaporation reaction.
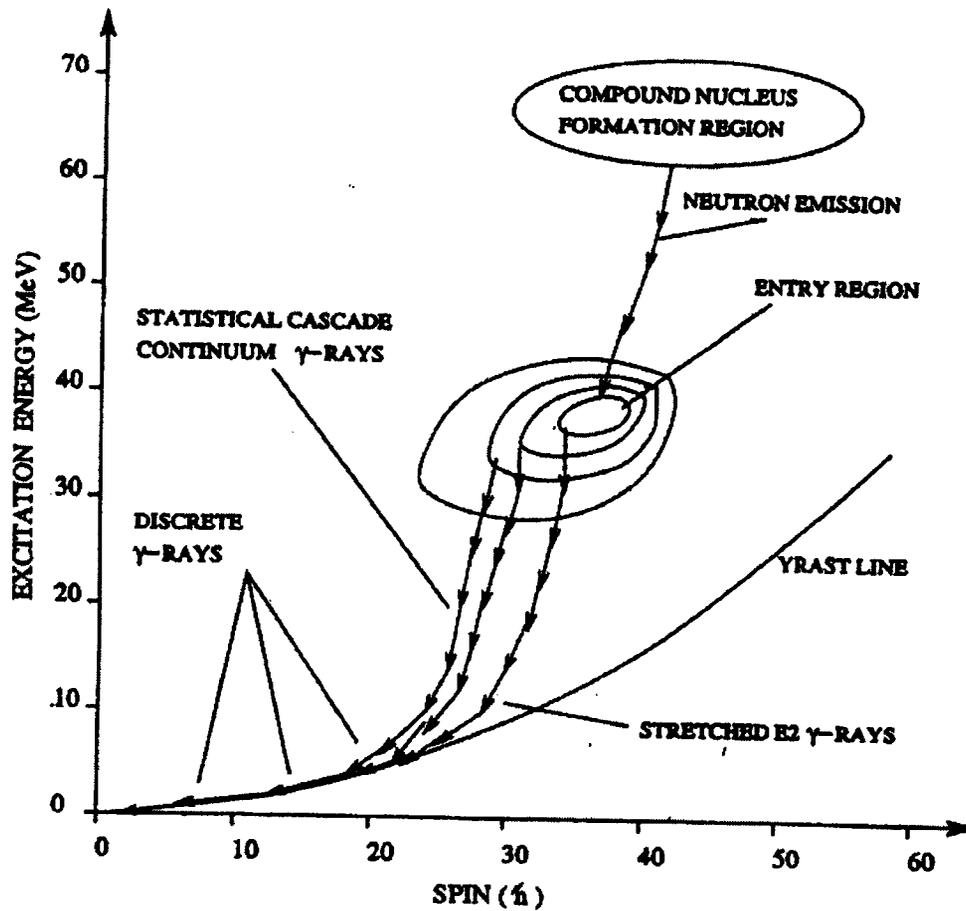
Figure 2.3: The deexcitation of the compound nucleus formed in heavy-ion fusion evaporation reaction.

2.4 Interaction of gamma rays with matter

Gamma rays interact with the detector crystal in three primary processes: The photoelectric effect, Compton scattering and pair production, see Fig. 2.4. These three processes are important because when gamma rays interact with the detector crystal they deposit some energy to the crystal. Below follows a brief description of each of these processes.

11
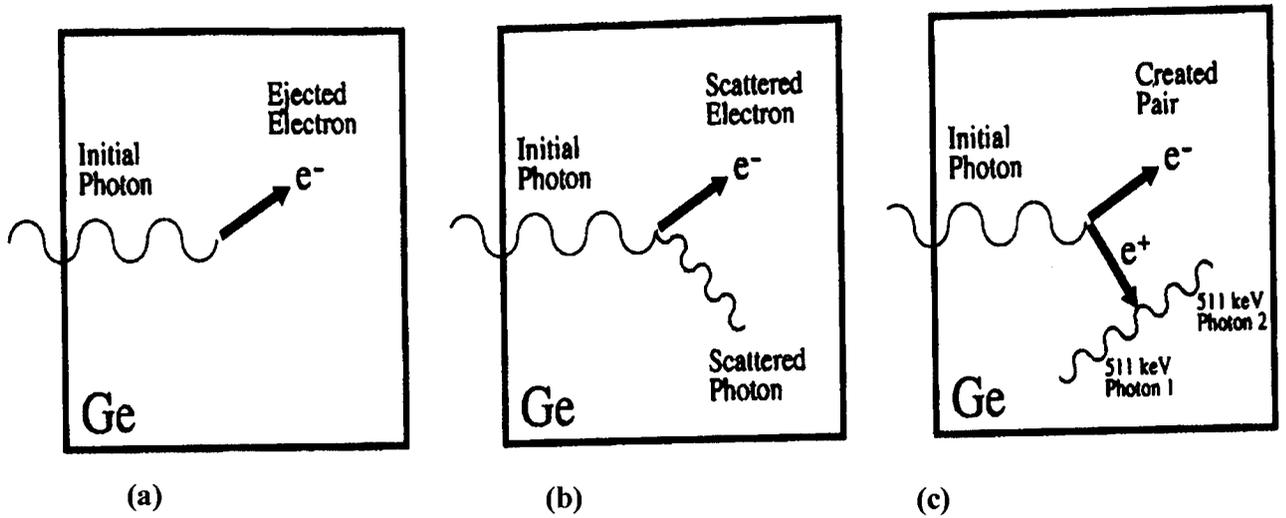
Figure 2.4: *The interaction of gamma rays in a germanium crystal follow three processes, namely, (a) photoelectric effect (left), (b) Compton scattering (center), and (c) pair production (right).*

2.4.1 Photoelectric Effect

The photoelectric effect occurs when the photon is totally absorbed by an atom. The photon energy minus the amount needed to free the electron is converted into the electron's kinetic energy;

$$T_e = E_\gamma - B_e \qquad (2.4)$$

Here B_e is the binding energy of the electron. The atom that has lost an electron may then de-excite by releasing other less tightly bound electrons. The most tightly bound electrons contribute more to photoelectric absorption (for $E_\gamma > B_K$, B_K is the binding energy of the K-shell electron). There is therefore a strong dependence on energy and atomic number Z. The photoelectric cross section is related to the atomic number and the γ-ray energy as follows:

$$\sigma \propto \frac{Z^n}{E_\gamma^m} \qquad (2.5)$$

Typical values for (n, m) are (3, 5). This process is dominant at photon energies less than 200keV. Fig. 2.5 shows the photoelectric effect cross-section dependence on the incident photon energy for Pb.
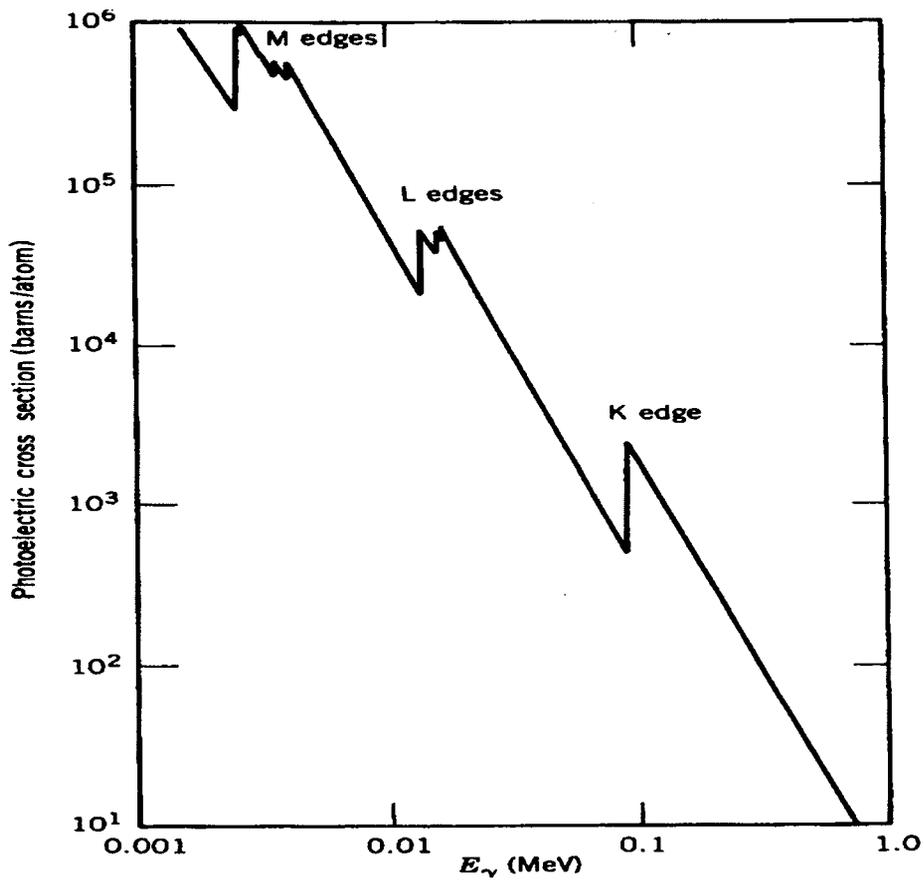
Figure 2.5: The photoelectric effect cross-section as a function of the incident photon energy for Pb [Kra88].

13

2.4.2 Compton scattering

Incoming gamma radiation can also undergo scattering in the detector crystal. Compton scattering plays an important role in the quality of the spectra produced. In Compton scattering a photon scatters from a nearly free atomic electron, resulting in a photon that is less energetic and a scattered electron carrying the energy lost by the photon. Energy conservation gives for the kinetic energy of the electron:

$$T = E_\gamma - E_\gamma' = E - m_0 c^2 \tag{2.6}$$

where E is the total energy of the recoil electron including its rest mass energy $m_0 c^2$, and E_γ and E_γ' are the energies of the incident photon and scattered photon, respectively. From the conservation of momentum and energy, the energy of the scattered photon is given by:

$$\frac{1}{E_\gamma'} - \frac{1}{E_\gamma} = \frac{1}{m_0 c^2}(1 - \cos\theta) \tag{2.7}$$

The probability for Compton scattering at an angle θ can be determined through quantum mechanical calculations, and the result is the Klein-Nishina formula for the differential cross section per electron. Compton scattering is sensitive to polarization: vertically polarized photons would be preferentially scattered in the horizontal plane. The Klein-Nishina formalism is also used to obtain the dependence of linear polarization on the Compton scattering. Fig. 2.6 shows that the Compton scattering cross-section is axially symmetric about the direction of incident photon with high energetic photons scattering in forward direction and low energy γ-rays scatter isotropically.

$$\frac{d\sigma}{d\Omega} = r_0^2 \left(\frac{E_\gamma'}{E_\gamma}\right)\left(\frac{E_\gamma'}{E_\gamma} + \frac{E_\gamma}{E_\gamma'} - 2\sin^2\zeta\cos^2\phi\right) \tag{2.8}$$

14

where r_0 is the classical electron radius equal to $\dfrac{e^2}{m_0c^2}$, m_0 is the electron mass, c the speed of light, ζ the Compton-scattering angle with respect to the direction of an incident gamma ray, and ϕ is the angle between its electric field and the Compton – scattering plane.
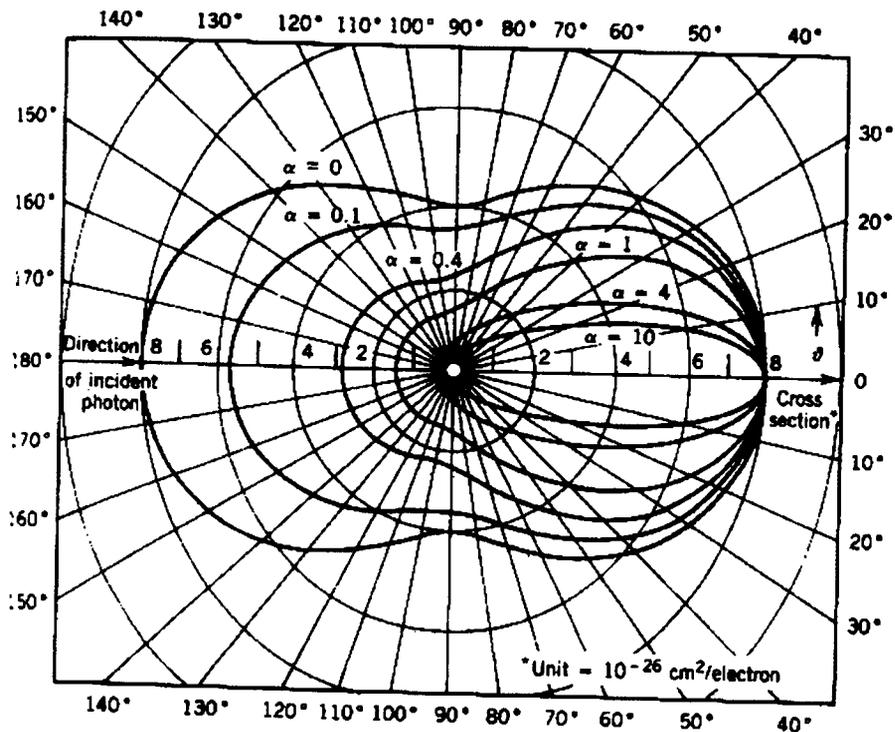
Figure 2.6: The Compton cross-section for various incident energies $\alpha = \dfrac{E}{m_0c^2}$ as calculated using the Klein-Nishina formalism and the Compton formula. The polar plot shows the intensity of the scattered radiation as a function of the scattering angle θ between the incident and scattered direction [Kra88].

15

2.4.3 Pair production

Pair production occurs when a γ-ray annihilates and results in the formation of a positron and an electron, and the γ-ray disappears in this process. The energy balance is given by:

$$E_\gamma = T_+ + mc^2 + T_- + mc^2$$ (2.9),

where T_+ and T_- are the energies of the positron and the electron respectively. The two particles have the individual rest mass energy of 511keV, and so pair production is not possible for γ-rays below 1022keV. Any excess energy is converted to the kinetic energy of the two created particles. The positron travels through the detector using its kinetic energy. Eventually when it slows down, it encounters an electron and the two annihilate each other, producing two 511keV γ-rays moving in opposite directions. This always occurs near an atomic nucleus. Pair production starts to compete with photoelectric effect for γ-rays in the MeV range see Fig. 2.7. From Fig. 2.7 it can be seen that, for example, for germanium ($Z = 32$) the photoelectric effect is dominant up to 200keV, while Compton scattering is dominant between 200keV and 1MeV. Pair production plays an important role for gamma ray energies above $E_\gamma \geq 1.5 MeV$.
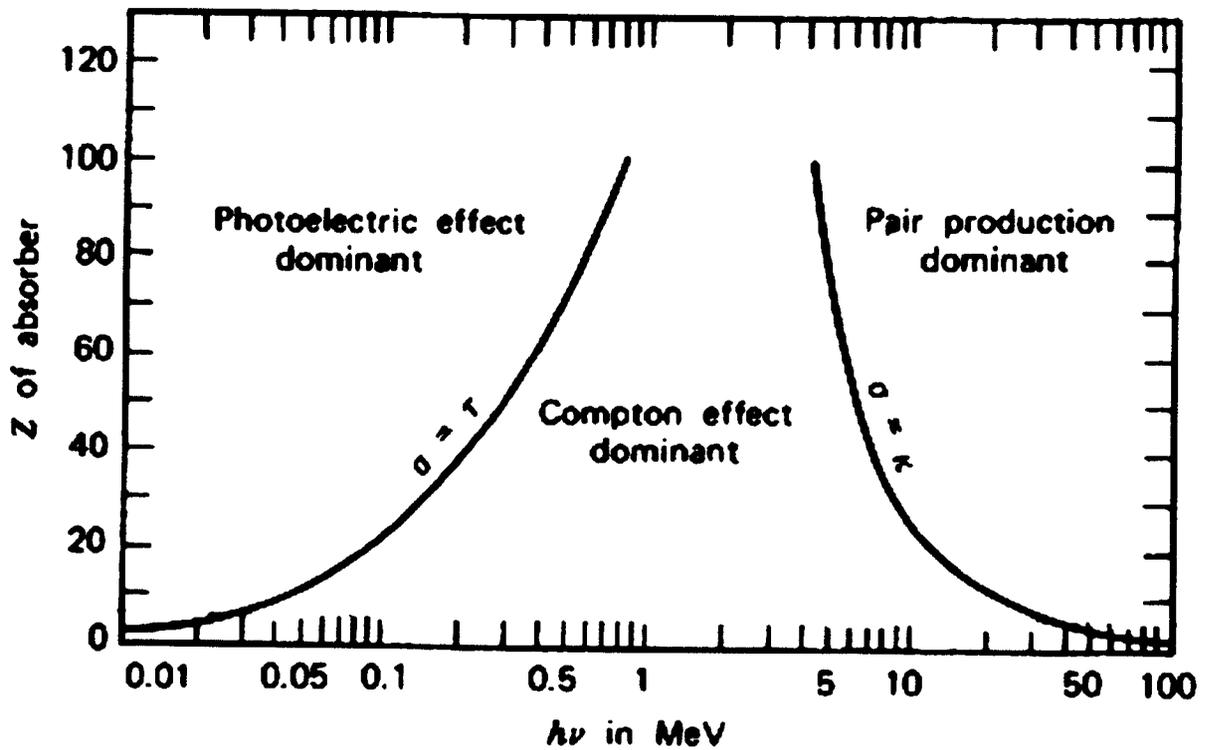
Figure 2.7: *Regions in which each of the three γ-ray interaction processes is dominant [Kra88].*

2.5 Correlations of gamma transitions

The multipolarity of γ-transitions and the relative spin and parities of the levels are usually determined by the measurement of angular distributions, angular correlations (DCO) and polarizations of γ-rays in heavy ion fusion evaporation reactions.

2.5.1 Angular distribution

The angular distributions $W(\theta)$ of γ-rays, is a measurement of the intensity of gamma transitions as a function of the angle θ with respect to the beam direction. In order to have an angular distribution, oriented nuclear states are required. Oriented means that the population of the m substates depends only on the magnitude of m, and not on its sign. To give a non-isotropic γ-ray angular distribution, relative population parameters $P(m)$ of the angular momentum substates have to be unequal, thus $P(m) \neq P(m')$, where m is the magnetic quantum number given by $m = -I,........+I$. $P(m)$ denotes the fraction of nuclei that occupy this state. The angular distribution of gamma rays emitted from such states has the form:

$$W(\theta) = \sum_k a_k P_k(\cos\theta) = a_0 P_0(\cos\theta) + a_2 P_2(\cos\theta) + a_4 P_4(\cos\theta) + ... \quad (2.10),$$

where a_k are coefficients of the corresponding Legendre Polynomials $P_k(\cos\theta)$ that depend upon the spins of the initial and final states from which the γ-ray transition originates and upon the multipolarity of the γ-ray transition. The quantity k takes even integer values only for conservation of parity, thus k = 0, 2, ...2I.

In heavy- ion fusion reactions, a Gaussian distribution of substates is formed with the population parameters $P(m)$ given by:

$$P(m) = \frac{e^{\frac{-m^2}{2\sigma^2}}}{\sum_{m'-I}^{I} e^{\frac{-m'^2}{2\sigma^2}}} \quad (2.11)$$

18

Here σ represents the width of the substate distribution. The angular distribution of γ-rays and the parameters accompanying the relation given in Equation 2.9 are well defined as explained in [Mor74].

2.5.2 Angular correlations

Angular correlation measurements involve the determination of the coincident intensities of two gamma rays in cascade detected at angles θ_1 and θ_2. Consider a situation where two gamma rays are in cascade from an initial state I_i to a final state I_f via an intermediate state, I as shown in the Fig. 2.8 below.
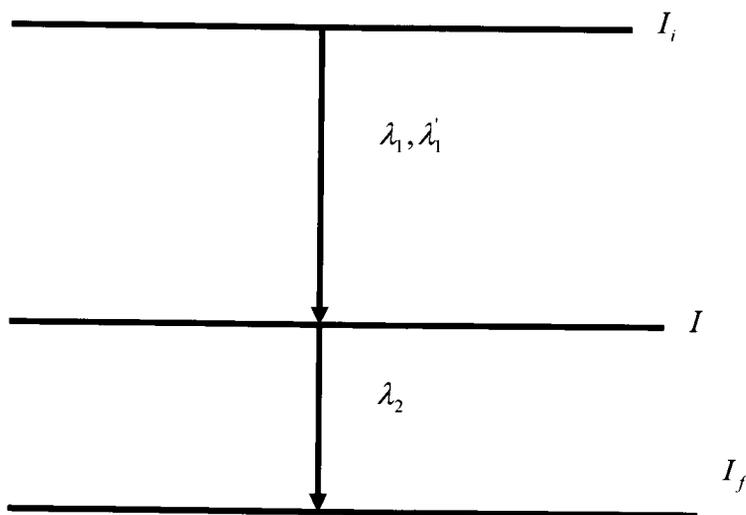
Figure 2.8: *Shows two successive gamma rays in cascade. The indices λ_1, λ_1' and λ_2 are multipole orders limited by spins and the multipolarities of gamma ray transitions. λ_1 , and λ_1' usually differ by 1 (like M1-E2), [Mor74].*

19

2.5.3 Directional correlations of gamma rays from oriented states (DCO)

The definition of DCO follows from two angular correlation functions, $W(\theta_1, \theta_2, \phi)$ and $W(\theta_2, \theta_1, \phi)$. DCO measurements determine λ, then λ is used to determine I_i if I_f is known, see Fig. 2.8. Therefore, the DCO ratio is defined as the ratio of two angular correlation functions:

$$R_{DCO} = \frac{W(\theta_1, \theta_2, \phi)}{W(\theta_2, \theta_1, \phi)} \tag{2.13}$$

Where $W(\theta_1, \theta_2, \phi)$ is the angular correlation of γ_1 detected at θ_1 in coincidence with γ_2 detected at θ_2, and $W(\theta_2, \theta_1, \phi)$ is the angular correlation of γ_1 detected at θ_2 in coincidence with γ_2 detected at θ_1. Fig. 2.10 depicts such correlation detection. The experimental R_{DCO} is given as:

$$R_{DCO} = \frac{I_{\theta_2}^{\gamma_1}(Gated_{\theta_1}^{\gamma_2})}{I_{\theta_1}^{\gamma_1}(Gated_{\theta_2}^{\gamma_2})} \tag{2.14}$$

Where $I_{\theta_2}^{\gamma_1}(Gated_{\theta_1}^{\gamma_2})$ is the intensity of γ_1 detected at θ_1 gated on γ_2 detected at θ_2 and $I_{\theta_1}^{\gamma_1}(Gated_{\theta_2}^{\gamma_2})$ is the intensity of γ_1 detected at θ_2 gated on γ_2 detected at θ_1. In the case of the AFRODITE array spectrometer the angles θ_1 and θ_2 are 135° or 45° and 90°. The angles 135° and 45° are treated as one angle because of symmetry. For the AFRODITE the angle ϕ is approximately 15° on average.
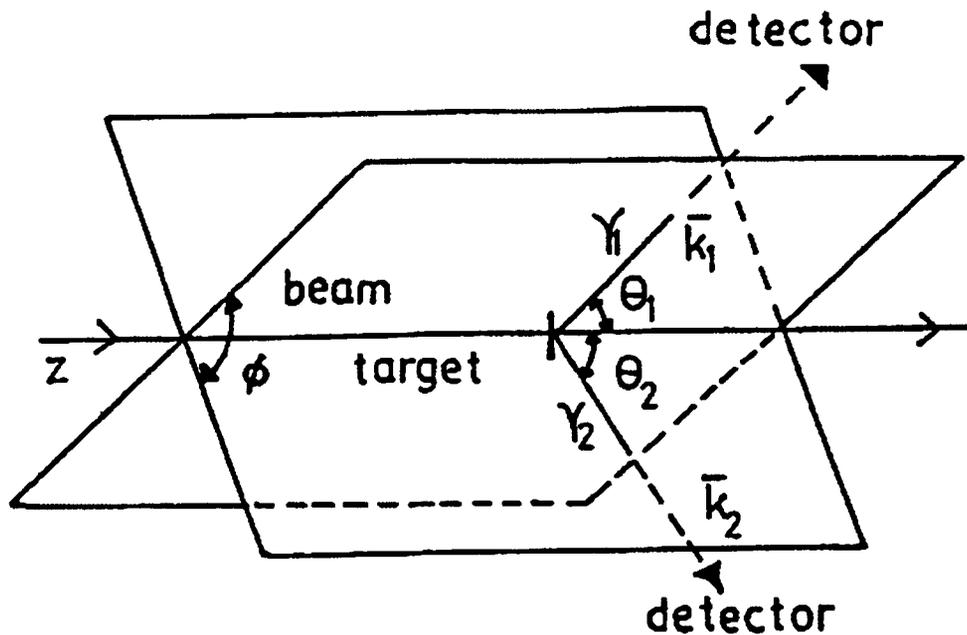
Figure 2.10: Shows setup for the correlation measurements of gamma rays.

2.5.4 Linear polarization measurements of gamma rays

Linear polarization measurements allow the magnetic (M) or electric (E) nature of gamma rays to be determined. Linear polarization measurements depend on Compton scattering of gamma rays, because the intensity of the scattered radiation depends on the direction of the electric field vector $\vec{E}$, as shown in Fig 2.11.

When γ-rays are linearly polarized, the angular distribution function of scattered γ-rays does not only depend on their outgoing direction θ with respect to the beam axis, but also on their electric field direction with respect to the reaction plane defined by an outgoing γ-ray and the beam axis, see Fig. 2.11. Since the linear polarization of γ-rays emitted from oriented states of nuclei has a close relation to their angular distribution, the linear polarization of these γ-rays in terms of their angular distribution functions is given by [Lee02]:

$$P(\theta) = \frac{W(\theta,\zeta = 0°) - W(\theta,\zeta = 90°)}{W(\theta,\zeta = 0°) + W(\theta,\zeta = 90°)}$$

(2.15)

Linear polarization of γ-rays is defined as the difference between the angular distribution function when their electric field is in or parallel to the reaction plane $W(\theta,\zeta = 0°)$, and when it is perpendicular to the reaction plane $W(\theta,\zeta = 90°)$, see Fig. 2.11. Here θ is the angle of the outgoing γ-rays with respect to the beam axis. Clover detectors can be used to perform linear polarization measurements. This detector can be used as both a scatterer to scatter incident γ-rays and an analyzer or a counter to detect γ-rays. This will help in measuring the number of γ-rays scattered perpendicular ($N_\perp$) and parallel ($N_{//}$) to the scattering plane. The difference between $N_\perp$ and $N_{//}$ with respect to the beam direction divided by their sum defines the polarization anisotropy as:

$$A_P = \frac{aN_\perp - N_{//}}{aN_\perp + N_{//}}$$

(2.16)

The normalization constant a can be found by taking the ratio of $N_\perp$ to $N_{//}$ for unpolarized γ-rays emitted from a standard calibration source and it also corrects for any instrumental effect between horizontal and vertical planes. The relation between $P(\theta)$ and A_P is given by:

$$A_P = Q_k P(\theta)$$

(2.17)

Here Q_k is the polarization sensitivity. In general, the polarization anisotropy has positive sign for stretched electric transitions and negative sign for stretched magnetic transitions, and the opposite for unstretched transitions. The Table 2.1 below shows the sign of linear polarization of γ-rays for different radiation types.

Table 2.1: Expected signs of a_2, a_4 and $P(\theta)$ for different radiation types. The values of a_2 and a_4 coefficients depend on the mixing ratio and the degree of alignment.

Radiation type	a_2	a_4	$P(\theta)$
Stretched M1	-	0	-
Unstretched M1	+	0	+
Stretched E1	-	0	+
Unstretched E1	+	0	-
Stretched M2	-	+	-
Stretched E2	+	-	+
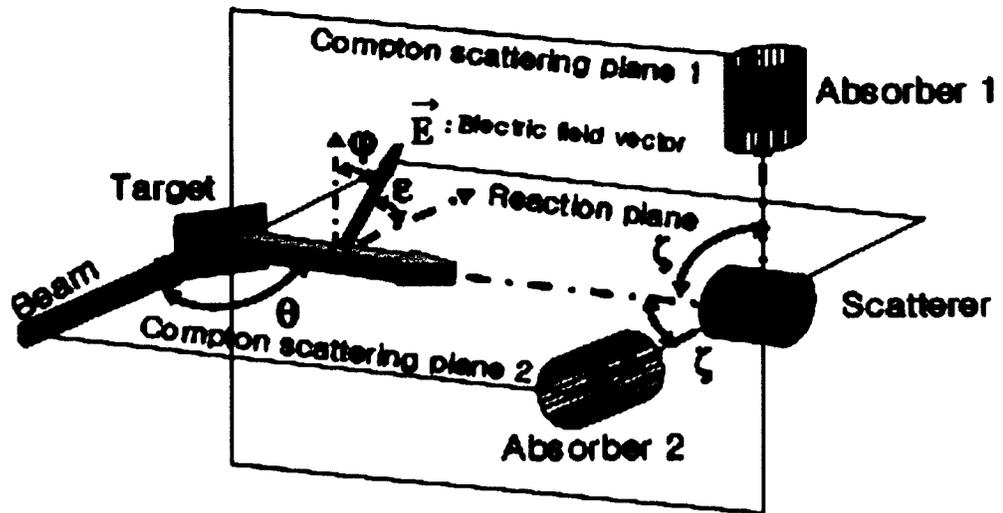
Figure 2.11: *Shows the setup showing linear polarization measurements of gamma rays.*

CHAPTER 3   EXPERIMENTAL DETAILS

3.1 AFRODITE array

When heavy ion fusion reactions are performed at iThemba Laboratory for Accelerator Based Sciences (LABS), gamma rays emitted from excited nuclei are detected by the AFRODITE[1] spectrometer array, see Fig. 3.1. It consists of two sets of high purity germanium (HPGe) detectors, namely, Clovers and Low Energy Photon Spectrometers (LEPS). Clover and LEPS detectors are situated at angles of 90°, 45° and 135° to the beam direction. The AFRODITE array design was based on the EXOGAM array; it has a rhombicuboctahedron shape with 18 square and 8 triangular facets, like that shown in Fig. 3.2. The two square facets situated at 0° and 180° accommodate the beam pipe. AFRODITE can hold a maximum of 16 detectors. All these detectors are maintained at liquid nitrogen temperature in their own cryostat. An automatic filling system fills the nitrogen dewars every 12 hours (current setup).

The AFRODITE array can also be used with ancillary detectors, such as the recoil detector, solar cells and DIAMANT. Both the latter are used to detect charged particles. The recoil detector uses the time taken for the reaction products to travel from the target to a carbon foil to discriminate between γ-rays emitted by the hot lighter fission products or from the heavier, slower residual nucleus. The recoil detector is run in coincidence with the AFRODITE. When AFRODITE is configured with 8 BGO-suppressed clovers in add-back mode and 7 LEPS, the total photopeak efficiency at 100keV is about 11%. However, at 1.3MeV it is only 1.5%, [Rou01]. This compares with 8% for Gammasphere, [Lie95].

---

[1] *AFRODITE is an acronym derived from AFRican Omnipurpose Detector for Innovative Techniques and Experiments.*
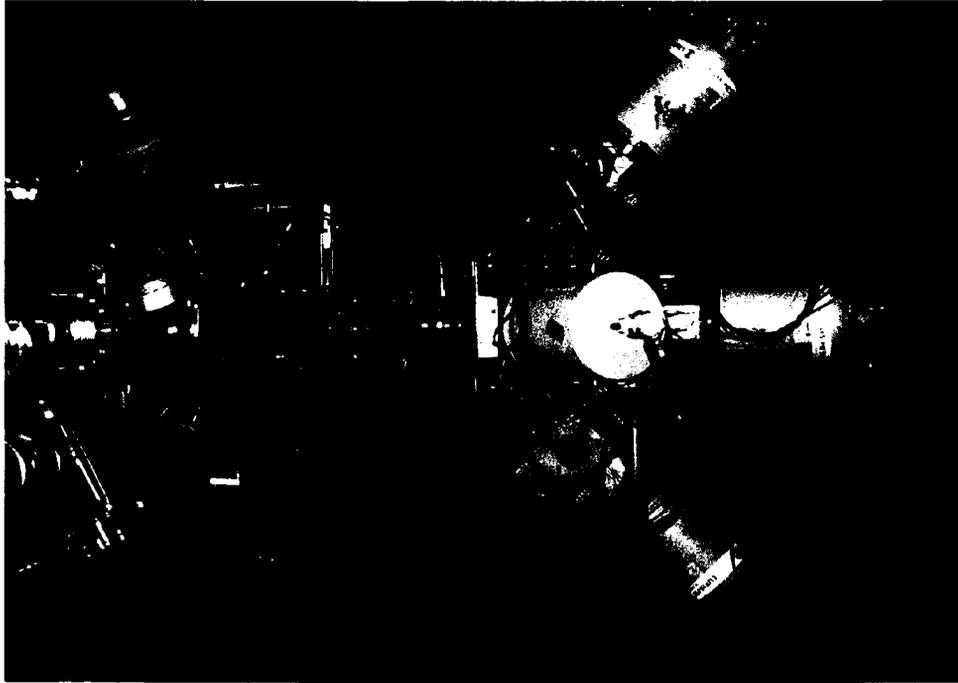
Figure 3.1: *AFRODITE array set up.*
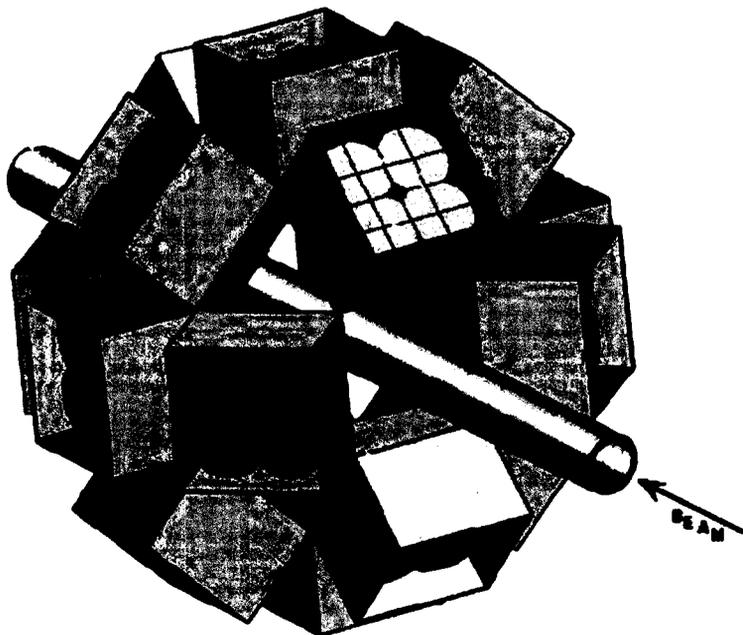
Figure 3.2: *Schematic drawing of the EXOGAM array, the design on which AFRODITE is based.*

27
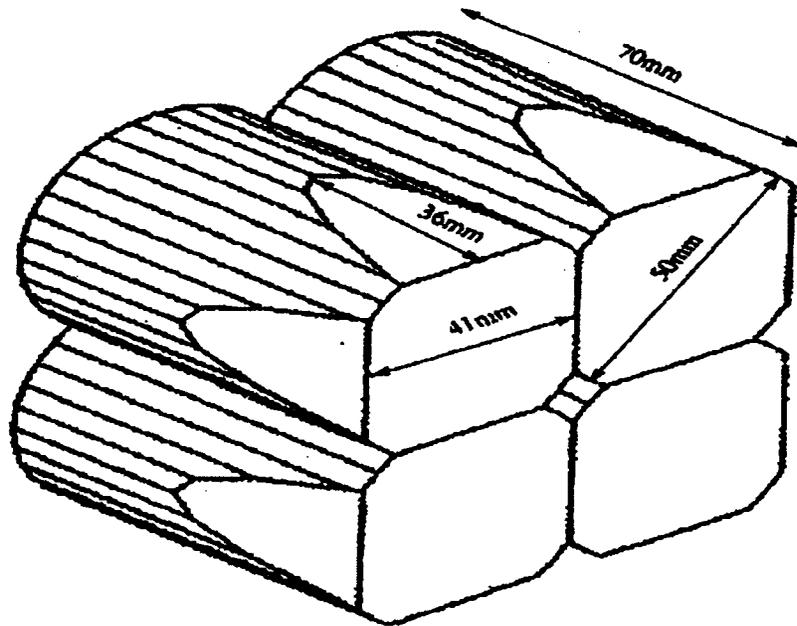
Figure 3.3: *A clover detector with the four-leaf HPGe crystals [Jon95].*

Figure 3.4: *A clover detector and its escape suppression shield [Duc99].*

3.2 (BGO)Background Compton suppression

The BGO Compton suppression shields are used to reduce the Compton background. Gamma-rays can either be fully absorbed by the detector or Compton scattered out of the detector. A γ-ray which escapes the Ge detector after Compton scattering will contribute to the unwanted background in the energy spectra. This happens to about 80% of the total events. By surrounding the Ge detector with a shield of highly efficient scintillation detectors (BGO) escaping gamma rays can be detected in order to reject the corresponding Ge detector signal. The BGO Compton suppression shield is run in anticoincidence with the Clovers. This means that if a γ ray interacts with both detector and shield, then the event will not be recorded. A figure of the BGO shield is shown in Fig. 3.4.

3.3 The Experiment

This experiment had already been performed when I started this project, and employed the AFRODITE array at iThemba LABS. A target of ^{152}Sm with a thickness of 5mg/cm^2 was bombarded with alpha beam energy of 45MeV. Excited states of ^{152}Gd were populated through the ^{152}Sm (^{4}He, 4n) ^{152}Gd fusion-evaporation reaction. The Separated-Sector Cyclotron (SSC) supplied the ^{4}He beam. The experiment was run over one weekend.

8 Clover detectors and 6 LEPS detectors of the AFRODITE array were used to detect the deexcitation γ-rays. These detectors were placed at angles of 135° and 90° to the beam direction. The trigger condition was such that at least two Clover detectors fired at the same time in order to accept the event. The MIDAS software DAQ package was used to record the data obtained in event-event mode. Standard ^{152}Eu and ^{133}Ba γ-ray sources were used to calibrate all these detectors. A total of 5x10^8 coincident events were collected.

CHAPTER 4 DATA ANALYSIS AND RESULTS

In order to build the level scheme of ^{152}Gd and assign spin and parity, several different two-dimensional data structures had to be constructed. These comprised the symmetric matrix for the level scheme, one asymmetric matrix for DCO measurements, and two asymmetric matrices for linear polarization measurements. The symmetric matrix and the level scheme had already been constructed by my co-supervisor by the time I started this project. My own role was to correct the gain drift of the Clover detectors, construct gamma-gamma asymmetric matrices for the measurements of DCO and linear polarization using the MIDAS sorting program, and then assign spin and parity in the ^{152}Gd decay scheme. Levels and γ-ray transitions, established thus far from our data are shown in Fig. 4.1 with spin and parity assigned.

Figure 4.1: *The* ^{152}*Gd decay scheme obtained from the* ^{152}*Sm* (^{4}*He, 4n*) ^{152}*Gd data.*

33
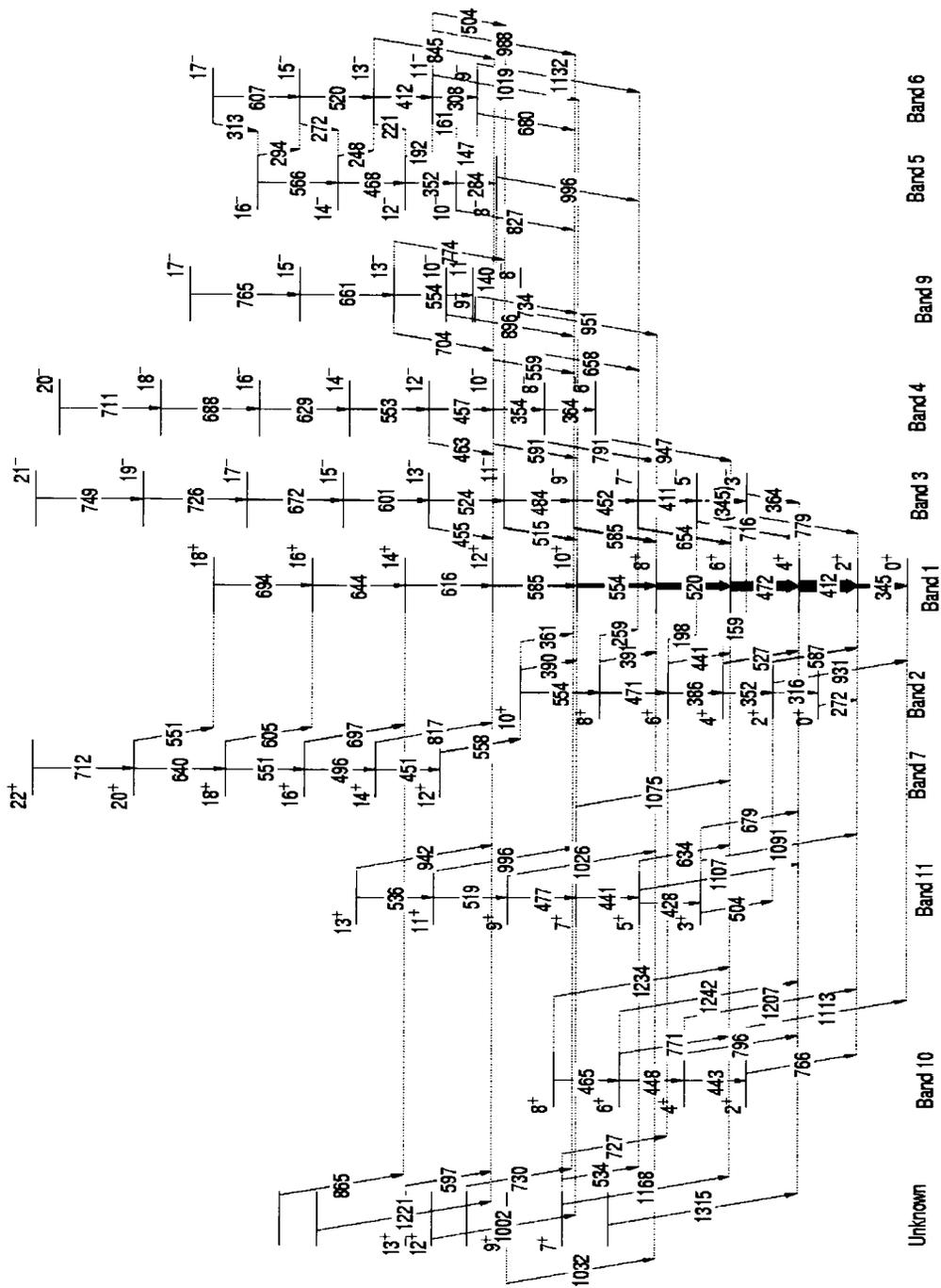
4.1 Energy calibration and gain matching

The energy calibration had been performed before I started this project. First of all source spectra for all AFRODITE detectors elements were acquired in singles mode using ^{152}Eu and ^{133}Ba sources. Then the program SFIT was used to find peak positions in each of the detector elements. After this, a quadratic expression $E = a_0 + a_1 x + a_2 x^2$ was used to fit the energy of the peaks as a function of channel number. The quadratic energy calibration equation $E = a_0 + a_1 x + a_2 x^2$, where x denotes channel number was mapped onto a linear energy equation $E = 0.5x'$ with x' channels as shown in Fig. 4.2. Mapping the two energy calibration equations yields:

$$0.5x' = a_0 + a_1 x + a_2 x^2$$
$$x' = 2a_0 + 2a_1 + 2a_2 x^2$$

(4.1)

The energy and efficiency calibrations were performed using ^{152}Eu and ^{133}Ba sources.
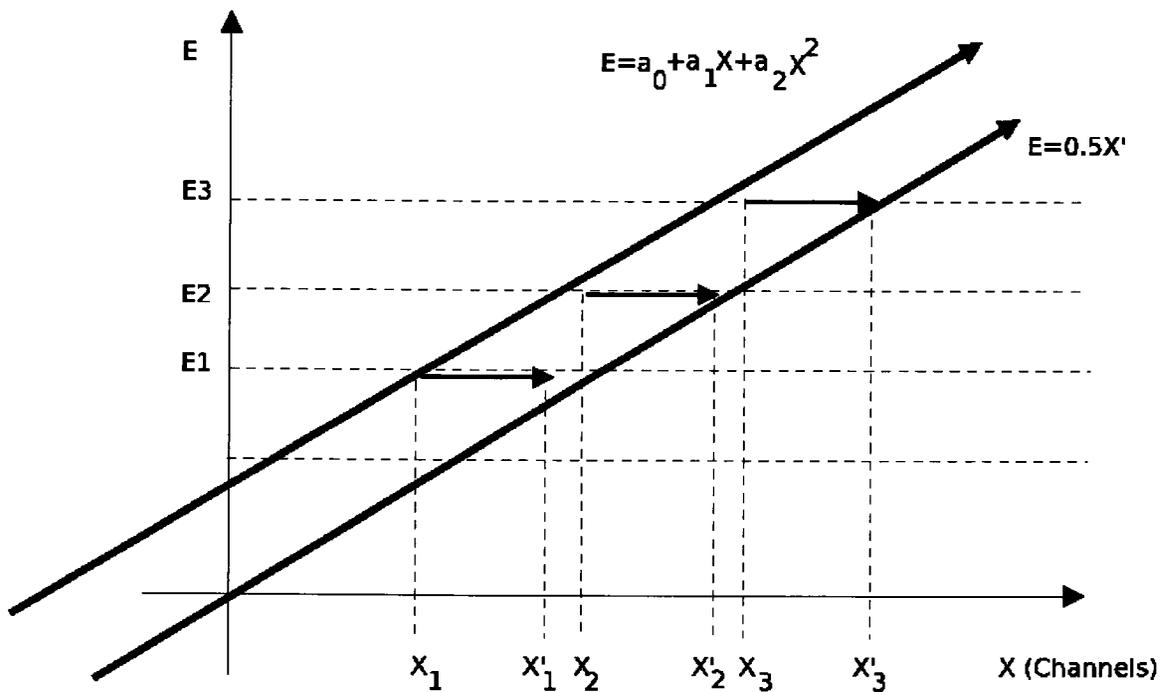
Figure 4.2: The mapping of the quadratic equation to the linear equation, [Mal06].

4.2 Efficiency calibration

When a gamma ray strikes a detector, it first undergoes interaction in the detector before detection takes place. Because of the distances between interactions, detectors are less than 100 percent efficient. Therefore it is important to have a precise figure for the detector efficiency in order to relate the number of pulses counted to the number of gamma rays incident on the detector. There are different types of efficiency defined for gamma-ray detectors, such as absolute efficiency, intrinsic efficiency, relative efficiency and photo peak or full-energy peak efficiency.

The absolute efficiency of a detector is defined as the ratio of the number of γ-rays detected by a detector to the number of γ-rays emitted from the source. Relative efficiency is the efficiency of one detector relative to another. Usually the relative efficiency of detectors is compared to that of a 3-in.-diameter by 3-in.-long NaI (Tl) detector at a distance of 25cm from the source. Intrinsic efficiency is the ratio of the number of γ-rays detected by the detector to the number of γ-rays that strikes it. Photopeak efficiency is the efficiency of detecting the full-energy of the γ-rays, that is peak events only. I used Radware to determine the relative efficiency curves for Clovers at 90° and 135°. The relative efficiency curves obtained using [133]Ba and [152]Eu sources are shown in Fig. 4.3. One curve for 90° Clovers and one for Clovers at 135°.
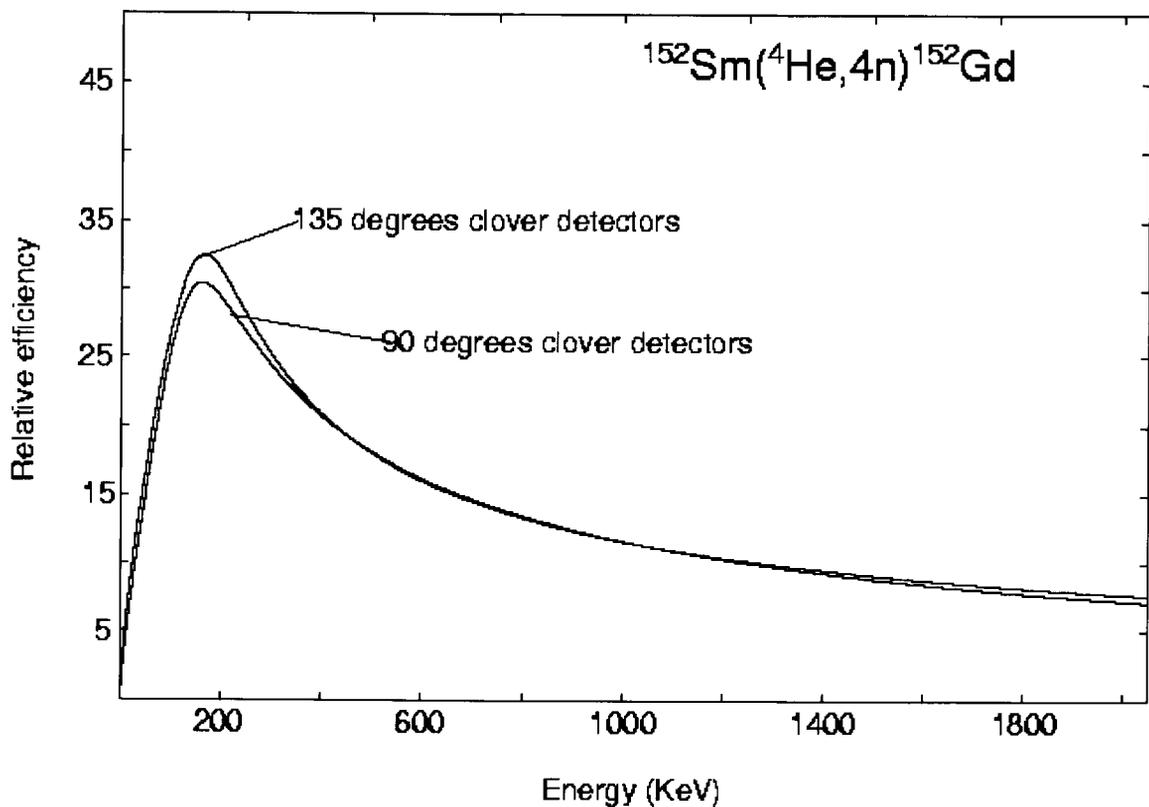
Figure 4.3: *The efficiency curve for the 90° and 135° clover detectors.*

$$R_{DCO} = \frac{I(135°,90°)}{I(90°,135°)}$$ (4.2),

where the numerator $I(135°,90°)$ is the intensity of γ_1 detected at 135° Clover detectors in coincidence with γ_2 detected at 90° Clover detectors, and the denominator $I(90°,135°)$ is the intensity of γ_1 detected at 90° Clover detectors in coincidence with γ_2 detected at 135° Clover detectors. The uncertainties in the measured R_{DCO} were calculated as follows:

$$\Delta R_{DCO} = R_{DCO} \sqrt{\left[\left(\frac{\Delta I(135°,90°)}{I(135°,90°)} \right)^2 + \left(\frac{\Delta I(90°,135°)}{I(90°,135°)} \right)^2 \right]}$$ (4.3),

where $\Delta I(135°,90°)$ and $\Delta I(90°,135°)$ are the uncertainties in the numerator and denominator measured using equation 4.3 above.
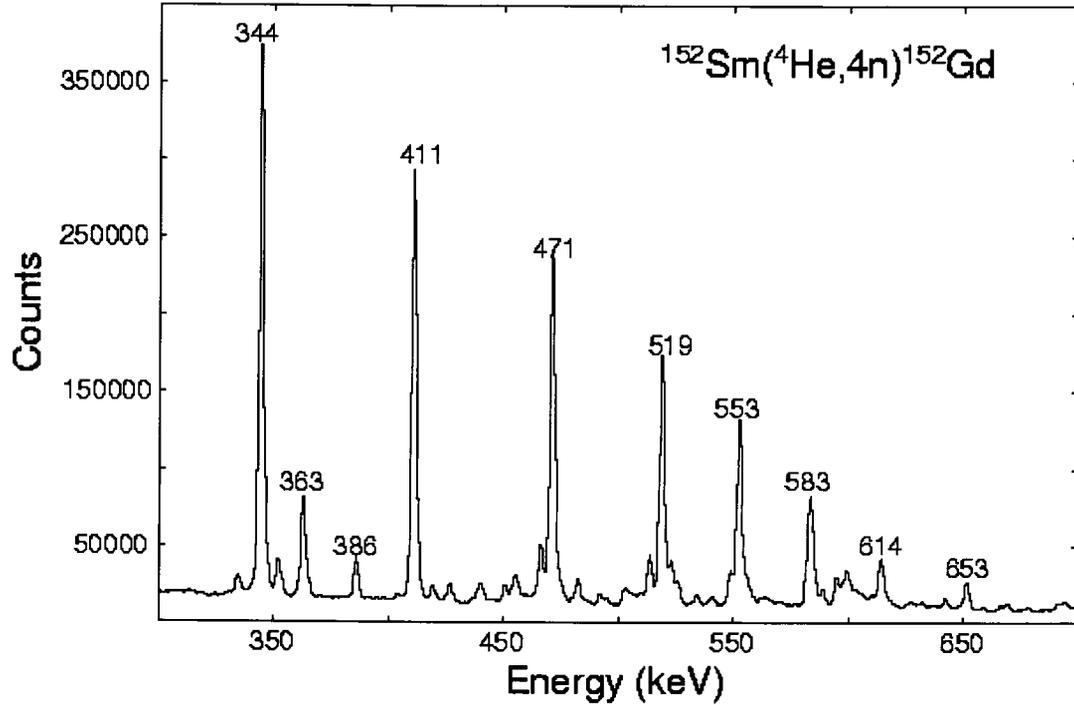
Figure 4.4: *The total projection spectrum of the matrix constructed for the measurements of R_{DCO} projected onto 135°. This matrix clearly shows the ground state band of the ^{152}Gd decay scheme.*

The index L is defined for electromagnetic radiation, so that 2^L is called the multipole order. This will give $L = 1$ for dipole, $L = 2$ for quadrupole, and so on. The R_{DCO} ratio depends on the multipolarity of the gating transition, the multipolarity of the transition in question and the configuration of the detector array. It also depends strongly on the mixing ratio (δ), see Fig. 4.5, and the alignment of nuclei. Fig. 4.5 shows that R_{DCO} strongly depend on the mixing ratio and that one R_{DCO} may correspond to two different δ. In the ratio σ/I, σ is the width of the gaussian peak and I is the spin. The alignment parameter σ / I increases with decreasing spin, see Fig. 4.6. If the width of the gaussian (σ) increases, the alignment decreases. Therefore one can expect DCO ratios to be less reliable at the lowest spins. The mixing ratio is given by:

$$\delta = \frac{\left\langle I_f \| \lambda' \| I_i \right\rangle}{\left\langle I_f \| \lambda \| I_i \right\rangle}$$ (4.4),

where λ and λ' are multipole orders as discussed in section 2.4.2, and I_i and I_f are the initial and final spins of gamma transitions respectively. Stretched dipole transitions are expected to lie at a ratio of ~0.61 (gating on $\Delta I = 2$), while stretched quadrupole transitions ($\Delta I = 2$) have a ratio of ~1 (gating on $\Delta I = 2$).
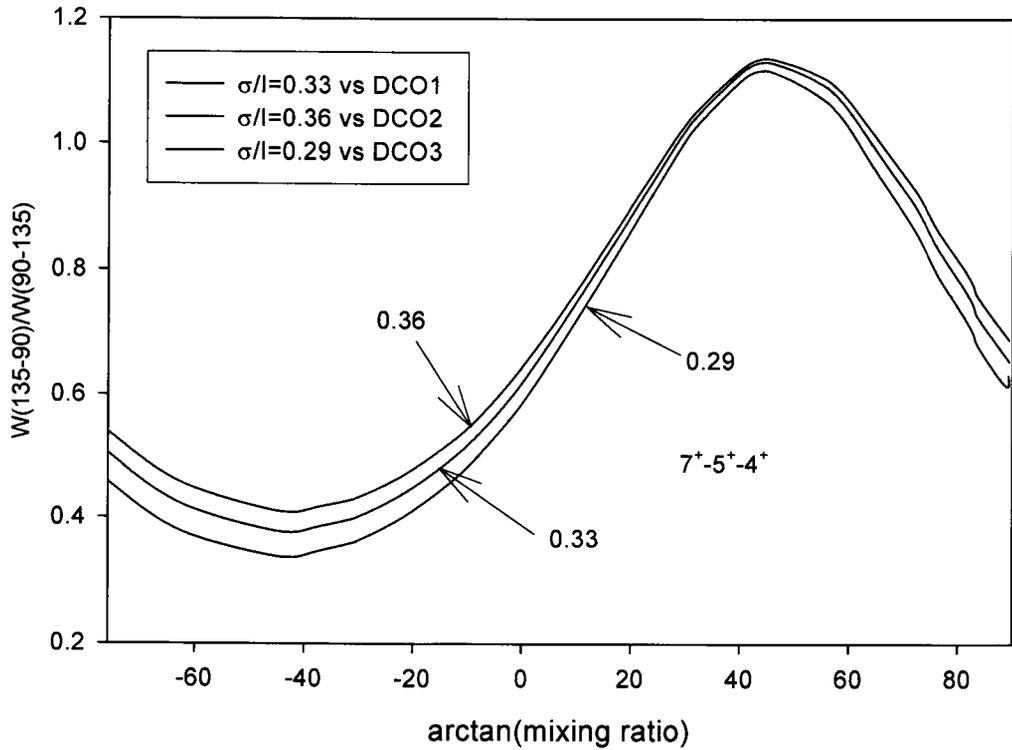
Figure 4.5: A plot showing the R_{DCO} values as a function of the mixing ratio [Mal06].
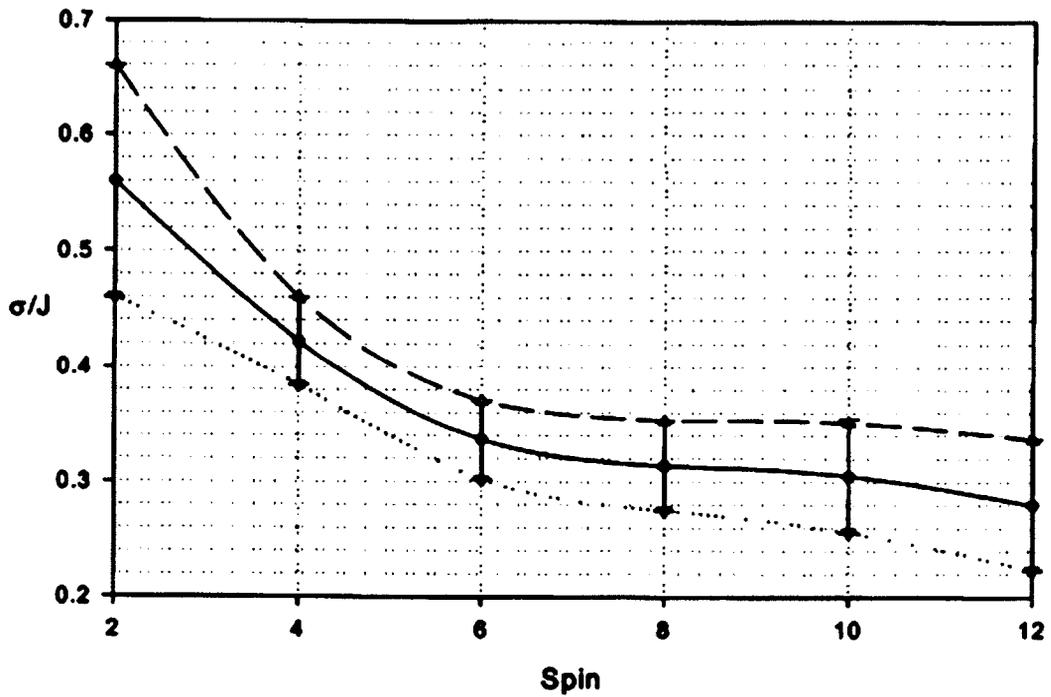
Figure 4.6: *Alignment as a function of spin, I [Bar08].In this figure, σ/j is the same as σ/I.*

The stretched dipole transitions have maximum intensity at 90° and their minimum at 180° with respect to the beam direction. The stretched quadrupole transitions have maximum intensity at 180° and their minimum at 90°, with respect to the beam direction as shown in Fig. 4.7.

41

intensity of stretched quadrupole transitions (520keV and 553keV) detected by Clovers at 135° is almost equal to that measured at 90°. The same gate shows that the intensity of stretched dipole transitions (515keV, 11^- → 10^+) detected by Clovers at 135° is less than that measured at 90°.

I also obtained some of my DCO results by setting gates on $\Delta I = 1$ stretched dipole transitions. An example of such a gate (set on the stretched $\Delta I = 1$ 654keV transition from 7^- → 6^+ in Band 3) is shown in Fig. 4.10. Fig. 4.11 summarizes the R_{DCO} of DCO analysis obtained by setting gates on $\Delta I = 1$ stretched dipole transitions. The average R_{DCO} setting gates on stretched dipole transition was found to be 0.95 (9). The DCO ratio does not depend on the electric or magnetic nature of a transition, therefore polarization measurements are needed for resolving spin and parity ambiguities.
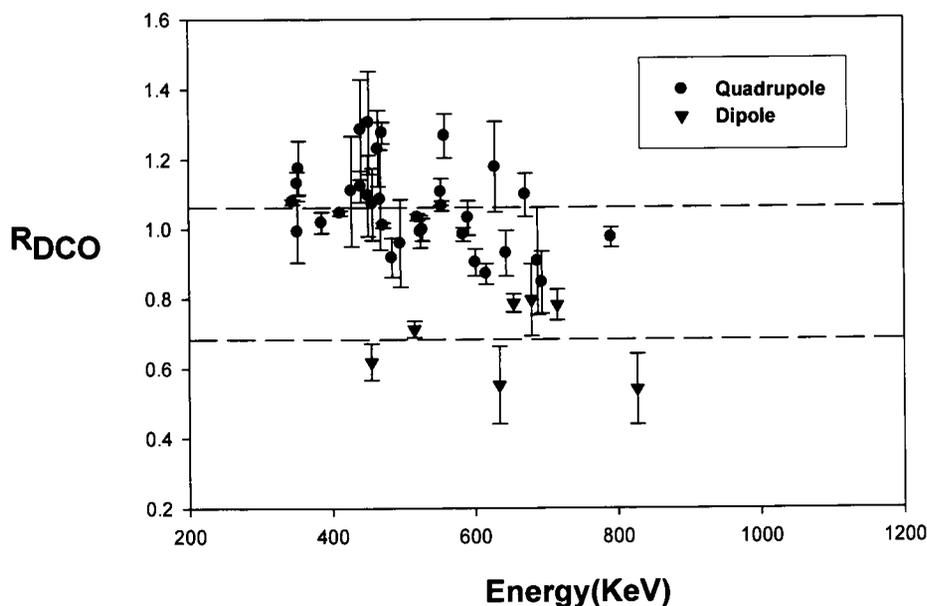
Figure 4.8: *This plot shows the R_{DCO} obtained from the DCO analysis gated on known stretched quadrupole transitions. The dashed lines indicate the average R_{DCO} obtained for quadrupole and dipole transitions.*

43

The other important factor that can cause this is the decay scheme of ^{152}Gd that is complicated by several strong doublets and multiplets. Furthermore, there are bands in the neighbouring nuclei, especially the complex decay scheme of ^{153}Gd, that have γ-rays very close in energy to those in bands in ^{152}Gd. This can cause some spin ambiguities in some of the transitions.
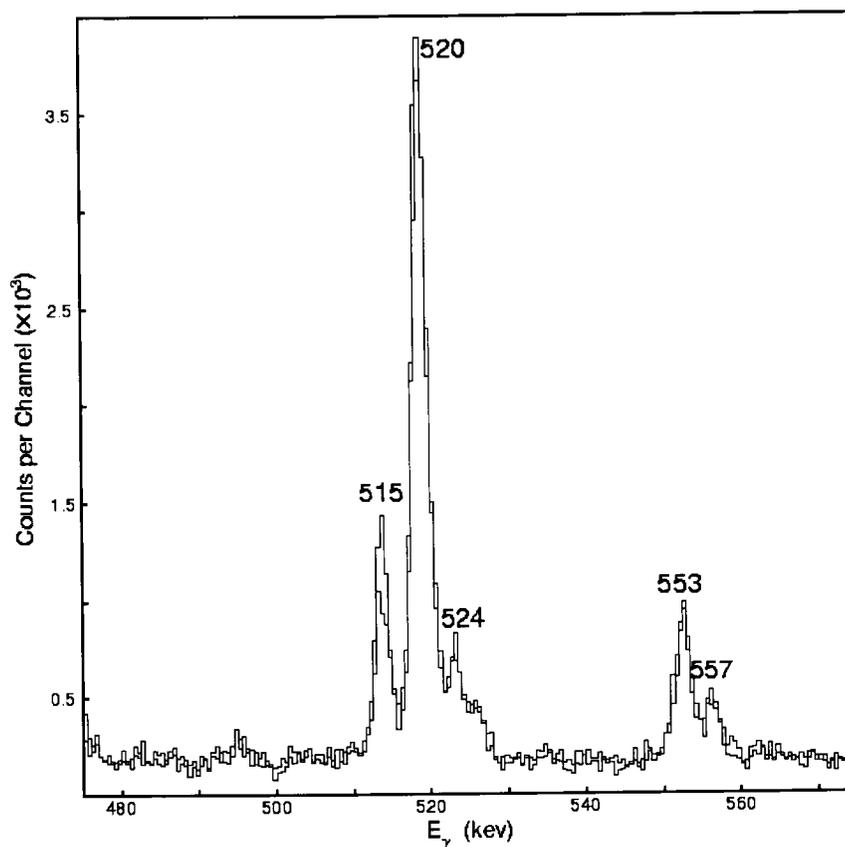
Figure 4.9: Gated spectra from the DCO matrix. The two spectra show the projections onto 90° and 135° axes respectively, when a gate is set on the 554keV transition ($10^+ \rightarrow 8^+$, stretched E2). In the case of the peak at 515keV the higher curve corresponds to Clovers at 90°, and the lower curve to Clovers at 135°.
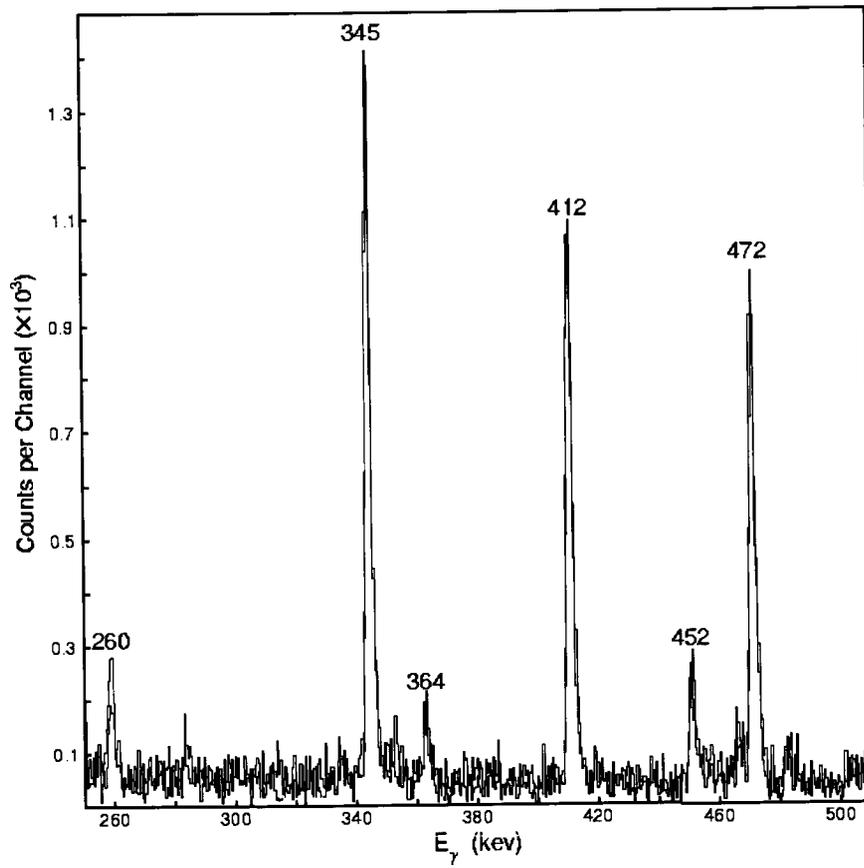
Figure 4.10: *A spectrum gate set on the stretched* $(7^- \rightarrow 6^+)$ *654keV transition. This figure shows the 90° and 135° projections superimposed.*
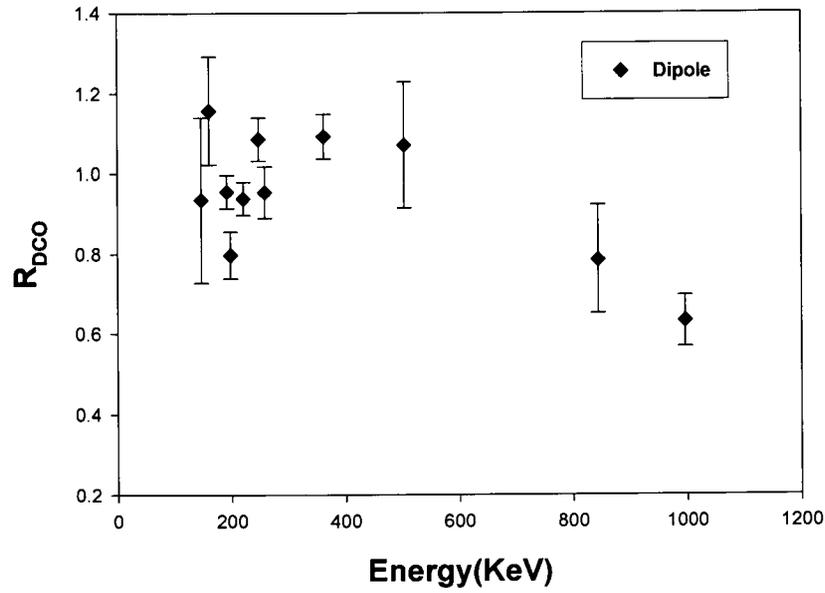
Figure 4.11: *The R_{DCO} obtained from the DCO analysis by setting gates on known stretched E1 transitions.*

4.5 Linear polarization analysis and results

The linear polarization anisotropies of γ-rays were deduced using only Clover detectors situated at 90° as suggested by [Twi73]. The experimental linear polarization anisotropy A_P of gamma transitions using the AFRODITE Clovers was measured as:

$$A_P = \frac{N_V - N_H}{N_V + N_H}$$

(4.5),

where N_V is the number of γ-rays that scattered perpendicular to the beam direction, and N_H is the number of γ-rays that scattered parallel to the beam direction as indicated in Fig. 4.12. The uncertainty in the A_p measured was calculated by using the equation:

$$\Delta A_p = \frac{2}{\left(N_V + N_H\right)^2} \sqrt{\left(N_H \sigma_V\right)^2 + \left(N_V \sigma_H\right)^2}$$ (4.6),

where σ_V and σ_H are the uncertainties in the number of γ-rays scattered vertically at 90° and horizontally at 90° clover detectors respectively.
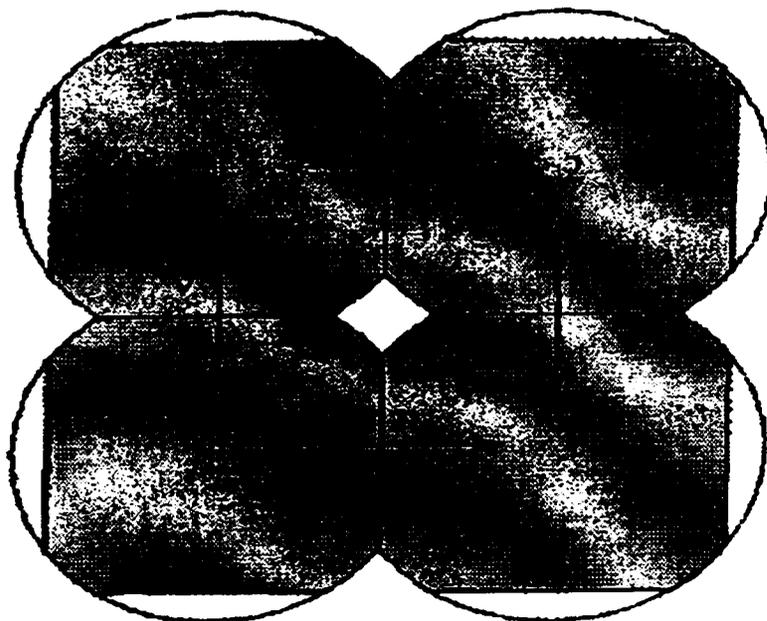
Figure 4.12: The horizontal and vertical scattering of gamma rays in a Clover detector.

In the case where there is little or no mixing, the polarization anisotropy is known to have positive sign for stretched electric transitions and negative sign for stretched magnetic transitions. It is just the opposite for unstretched transitions. For mixed, $\Delta I = 1$, M1/E2 transitions the linear polarization $P(\theta)$ also depends on the mixing ratio. A single $P(\theta)$ value may correspond to more than one value of δ, [Twi73]. Fig. 4.13 shows the linear polarization $P(\theta)$ values as a function of the mixing ratio. When δ is zero, it means that there is no mixing and that corresponds to pure M1 transition. Pure E2 corresponds to $\delta = 90°$. The Figure 4.14 summarizes results obtained for the linear polarization anisotropy measurements in the current work.

$$I_{initial} = 12 \quad (\sigma/I=0.3)$$
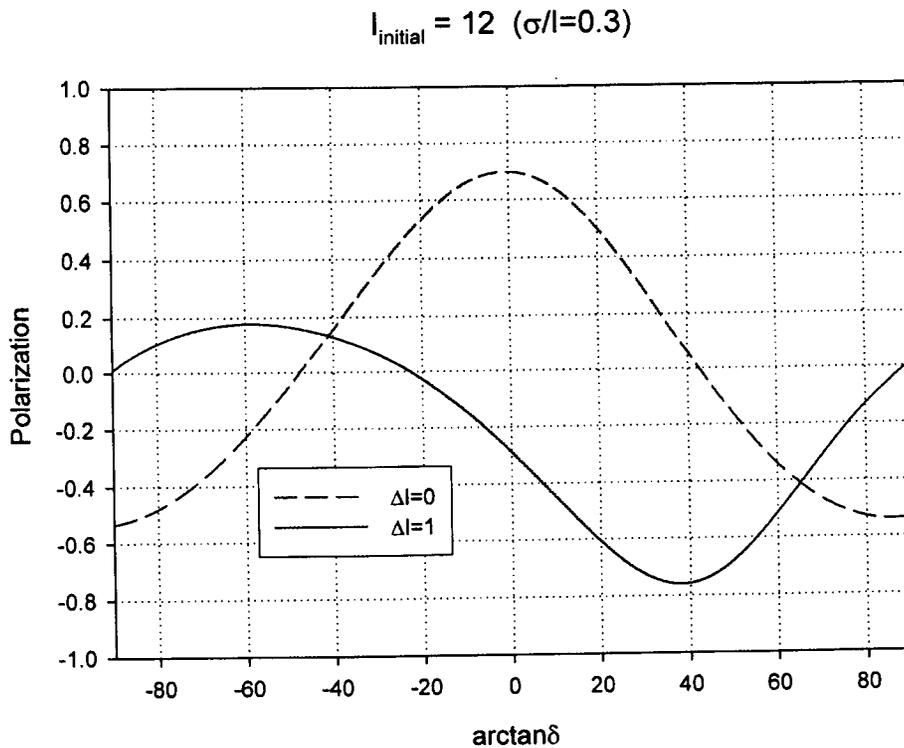
Figure 4.13: A plot of linear polarization $P(\theta)$ as a function of the mixing ratio for mixed M1/E2 transitions. The doted line indicates the plot for $\Delta I = 0$ transitions, and the solid line indicates the plot for $\Delta I = 1$ transitions, [Bar08].
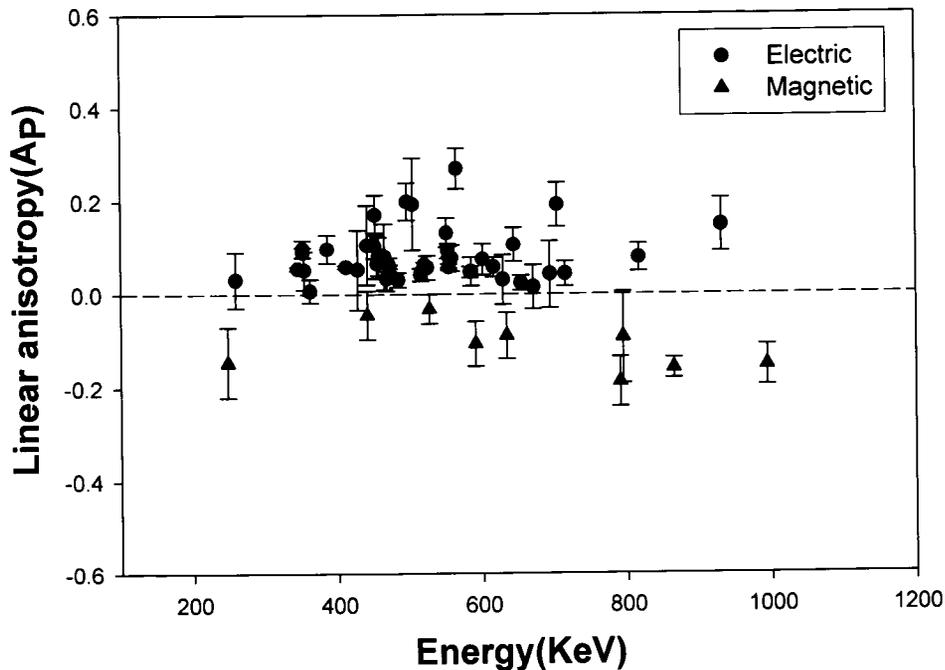
Figure 4.14: The polarization anisotropy results obtained.

With the present matrices the value of the polarization anisotropy does not depend on the multipolarity of the gating transition. Both known stretched E1 and E2 transitions were therefore used as gating transitions. We observed that the difference between the vertical coincidence spectrum and the horizontal coincidence spectrum show that the electric transitions have positive counts and the magnetic transitions have negative counts. Electric transitions have negative counts and magnetic transitions have positive counts when the vertical coincidence spectrum is subtracted from the horizontal coincidence spectrum. The polarization results combined with the DCO results will allow spin and parity assignments of the energy levels in the nucleus ^{152}Gd.

Tables showing DCO, linear polarization anisotropy and multipolarity assigned for γ-ray transitions in different bands of the ^{152}Gd decay scheme follow below. Discussions for spin and parity assignments follow in the next chapter.

49

Table 4.1: *Gamma-ray energies, R_{DCO} ratios (gated on $\Delta I = 2$ transitions), and polarization anisotropy (A_p) and the multipolarity assigned to gamma transitions in the ^{152}Gd decay scheme.*

Band 1:

$E_\gamma\,(keV)$	$I_i^\pi \rightarrow I_f^\pi$	R_{DCO}	A_P	Multipolarity
345	$2^+ \rightarrow 0^+$	1.08(1)	0.05(1)	E2
412	$4^+ \rightarrow 2^+$	1.05(1)	0.06(1)	E2
472	$6^+ \rightarrow 4^+$	1.01(1)	0.06(1)	E2
520	$8^+ \rightarrow 6^+$	1.03(1)	0.06(1)	E2
554	$10^+ \rightarrow 8^+$	1.07(1)	0.06(1)	E2
584	$12^+ \rightarrow 10^+$	0.98(2)	0.05(1)	E2
616	$14^+ \rightarrow 12^+$	0.87(3)	0.06(2)	E2
644	$16^+ \rightarrow 14^+$	0.93(7)	0.11(4)	E2
694	$18^+ \rightarrow 16^+$	0.85(9)	0.04(4)	E2

Table 4.2: *Gamma-ray energies, R_{DCO} ratios (gated on $\Delta I = 2$ transitions in the ground state band), polarization anisotropy (A_p) and the multipolarity assigned to gamma transitions in the ^{152}Gd decay scheme. The R_{DCO} for the 198keV, 259keV and 362keV transitions was determined by setting gates on stretched dipole ($\Delta L = 1$) transitions.*

Band 2:

$E_\gamma(keV)$	$I_i^\pi \to I_f^\pi$	R_{DCO}	A_p	Multipolarity
316	$2^+ \to 0^+$	)^a	)^a	)^b
352	$4^+ \to 2^+$	1.13(4)	0.10(2)	E2
386	$6^+ \to 4^+$	1.02(3)	0.10(3)	E2
471	$8^+ \to 6^+$	1.28(3)	0.06(1)	E2
554	$10^+ \to 8^+$	1.04(2)	0.08(2)	E2
272	$0^+ \to 2^+$	)^a	)^a	)^b
931	$2^+ \to 0^+$	)^a	0.15(6)	E2
587	$2^+ \to 2^+$	)^a	)^a	)^b
527	$4^+ \to 4^+$	1.00(3)	-0.03(3)	E2
441	$6^+ \to 6^+$	1.12(5)	-0.04(5)	E2
159	$4^+ \to 3^-$	)^a	)^a	)^b
198	$6^+ \to 5^-$	0.80(6))^c	0.06(7)	E1
259	$8^+ \to 7^-$	0.95(7))^c	0.03(6)	E1
361	$10^+ \to 9^-$	1.09(6))^c	0.01(2)	E1

)^a insufficient statistics to measure gamma-ray intensity.

)^b Multipolarity could not be determined.

)^c DCO ratio obtained by gating on stretched dipole

Table 4.3: Gamma-ray energies, R_{DCO} ratios (gated on $\Delta I = 2$ transitions), and polarization anisotropy (A_p) and the multipolarity assigned to gamma transitions in the ^{152}Gd decay scheme.

Band 3:

$E_\gamma (keV)$	$I_i^\pi \to I_f^\pi$	R_{DCO}	A_p	Multipolarity
345	$5^- \to 3^-$	$)^a$	$)^a$	$)^b$
411	$7^- \to 5^-$	$)^a$	$)^a$	$)^b$
452	$9^- \to 7^-$	1.31(15)	0.17(4)	E2
484	$11^- \to 9^-$	0.92(6)	0.03(2)	E2
524	$13^- \to 11^-$	0.99(5)	0.06(3)	E2
601	$15^- \to 13^-$	0.90(4)	0.07(3)	E2
672	$17^- \to 15^-$	1.10(6)	0.01(5)	E2
726	$19^- \to 17^-$	$)^a$	$)^a$	$)^b$
749	$21^- \to 19^-$	$)^a$	$)^a$	$)^b$
364	$3^- \to 4^+$	$)^a$	$)^a$	$)^b$
779	$3^- \to 2^+$	$)^a$	$)^a$	$)^b$
715	$5^- \to 4^+$	0.78(4)	0.04(3)	E1
654	$7^- \to 6^+$	0.79(3)	0.02(2)	E1
585	$9^- \to 8^+$	$)^a$	0.05(3)	E1
515	$11^- \to 10^+$	0.71(2)	0.04(1)	E1
455	$13^- \to 12^+$	0.62(5)	0.07(3)	E1

$)^a$ insufficient statistics to measure gamma-ray intensity.
$)^b$ multipolarity could not be determined.

Table 4.4: *Gamma-ray energies, R_{DCO} ratios (gated on $\Delta I = 2$ transitions), and polarization anisotropy (A_P) and the multipolarity assigned to gamma transitions in the ^{152}Gd decay scheme.*

Band 4:

$E_\gamma (keV)$	$I_i^\pi \rightarrow I_f^\pi$	R_{DCO}	A_P	Multipolarity
364	$8^- \rightarrow 6^-$	1.18(5)	)^a	)^b
354	$10^- \rightarrow 8^-$	1.18(8)	0.05(4)	E2
457	$12^- \rightarrow 10^-$	1.07(10)	0.08(4)	E2
553	$14^- \rightarrow 12^-$	1.11(4)	0.09(2)	E2
629	$16^- \rightarrow 14^-$	1.18(13)	0.03(5)	E2
688	$18^- \rightarrow 16^-$	0.91(29)	)^a	)^b
711	$20^- \rightarrow 18^-$	)^a	)^a	)^b
947	$6^- \rightarrow 6^+$	)^a	)^a	)^b
791	$8^- \rightarrow 8^+$	0.98(3)	-0.19(5)	E1
591	$10^- \rightarrow 10^+$	1.03(5)	-0.11(5)	E1
463	$12^- \rightarrow 12^+$	)^a	)^a	)^b
559	$10^- \rightarrow 9^-$	)^a	)^a	)^b
658	$8^- \rightarrow 7^-$	)^a	)^a	)^b

)^a insufficient statistics to measure gamma-ray intensity.

)^b multipolarity could not be determined.

Table 4.5: *Gamma-ray energies, R_{DCO} ratios (gated on $\Delta I = 2$ transitions), and polarization anisotropy (A_P) and the multipolarity assigned to gamma transitions in the ^{152}Gd decay scheme.*

Band 5:

$E_\gamma (keV)$	$I_i^\pi \rightarrow I_f^\pi$	R_{DCO}	A_P	Multipolarity
284	$10^- \rightarrow 8^-$	$)^a$	$)^a$	$)^b$
352	$12^- \rightarrow 10^-$	0.99(9)	0.09(1)	E2
468	$14^- \rightarrow 12^-$	1.09(14)	0.03(3)	E2
566	$16^- \rightarrow 14^-$	1.09(16)	0.27(4)	E2
996	$8^- \rightarrow 7^-$	$0.63(6))^c$	-0.057(4)	M1/E2
827	$10^- \rightarrow 9^-$	$0.54(10))^c$	-0.01(8)	M1/E2
147	$10^- \rightarrow 9^-$	0.93(21)	$)^a$	$)^b$
192	$12^- \rightarrow 11^-$	0.9594)	-0.06(8)	M1/E2
248	$14^- \rightarrow 13^-$	1.09(5)	-0.15(7)	M1/E2
294	$16^- \rightarrow 15^-$	$)^a$	$)^a$	$)^b$

$)^a$ insufficient statistics to measure gamma-ray intensity.

$)^b$ multipolarity could not be determined.

$)^c$ DCO ratio obtained by gating on stretched dipole

Table 4.6: *Gamma-ray energies, R_{DCO} ratios (gated on $\Delta I = 2$ transitions), and polarization anisotropy (A_p) and the multipolarity assigned to gamma transitions in the ^{152}Gd decay scheme.*

Band 6:

$E_\gamma(keV)$	$I_i^\pi \to I_f^\pi$	R_{DCO}	A_P	Multipolarity
308	$11^- \to 9^-$	)^a	)^a	)^b
412	$13^- \to 11^-$	)^a	)^a	)^b
520	$15^- \to 13^-$	)^a	)^a	)^b
607	$17^- \to 15^-$	)^a	)^a	)^b
161	$11^- \to 10^-$	1.16(13)	)^a	)^b
221	$13^- \to 12^-$	0.94(4)	-0.02(14)	M1/E2
272	$15^- \to 14^-$	1.26(16)	)^a	)^b
313	$17^- \to 16^-$	)^a	)^a	)^b
680	$9^- \to 9^-$	)^a	)^a	)^b
1019	$11^- \to 10^+$	)^a	)^a	)^b
1132	$9^- \to 7^-$	)^a	)^a	)^b
988	$11^- \to 9^-$	)^a	)^a	)^b
504	$11^- \to 11^-$	1.07(16)	-0.19(10)	M1/E2
845	$13^- \to 12^+$	0.79(14)	0.07(9)	E1

)^a insufficient statistics to measure gamma-ray intensity.

)^b multipolarity could not be determined.

Table 4.7: *Gamma-ray energies, R_{DCO} ratios (gated on $\Delta I = 2$ transitions), and polarization anisotropy (A_P) and the multipolarity assigned to gamma transitions in the ^{152}Gd decay scheme.*

Band 7:

$E_\gamma(keV)$	$I_i^\pi \rightarrow I_f^\pi$	R_{DCO}	A_P	Multipolarity
451	$14^+ \rightarrow 12^+$	1.10(12)	0.10(3)	E2
496	$16^+ \rightarrow 14^+$	0.96(13)	0.20(3)	E2
551	$18^+ \rightarrow 16^+$	)^a	0.13(3)	E2
640	$20^+ \rightarrow 18^+$	)^a	)^a	)^b
558	$12^+ \rightarrow 10^+$	1.27(6)	0.08(3)	E2
817	$14^+ \rightarrow 12^+$	)^a	0.08(3)	E2
697	$16^+ \rightarrow 14^+$	)^a	)^a	)^b
605	$18^+ \rightarrow 16^+$	)^a	)^a	)^b
551	$20^+ \rightarrow 18^+$	)^a	)^a	)^b

)^a insufficient statistics to measure gamma-ray intensity.

)^b multipolarity could not be determined.

Table 4.8: *Gamma-ray energies, R_{DCO} ratios (gated on $\Delta I = 2$ transitions), and polarization anisotropy (A_P) and the multipolarity assigned to gamma transitions in the ^{152}Gd decay scheme.*

Band 9:

$E_\gamma (keV)$	$I_i^\pi \rightarrow I_f^\pi$	R_{DCO}	A_P	Multipolarity
554	$13^- \rightarrow 11^-$	$)^a$	$)^a$	$)^b$
661	$15^- \rightarrow 13^-$	$)^a$	$)^a$	$)^b$
765	$17^- \rightarrow 15^-$	$)^a$	$)^a$	$)^b$
951	$8^- \rightarrow 8^+$	$)^a$	$)^a$	$)^b$
734	$11^- \rightarrow 10^+$	$)^a$	$)^a$	$)^b$
896	$10^- \rightarrow 9^-$	$)^a$	$)^a$	$)^b$
704	$13^- \rightarrow 12^+$	$)^a$	0.19(5)	$)^b$
910	$15^- \rightarrow 13^-$	$)^a$	$)^a$	$)^b$
774	$13^- \rightarrow 11^-$	$)^a$	$)^a$	$)^b$

$)^a$ insufficient statistics to measure gamma-ray intensity.

$)^b$ multipolarity could not be determined.

Table 4.9: *Gamma-ray energies, R_{DCO} ratios (gated on $\Delta I = 2$ transitions), and polarization anisotropy (A_P) and the multipolarity assigned to gamma transitions in the ^{152}Gd decay scheme.*

Band 10:

$E_\gamma (keV)$	$I_i^\pi \rightarrow I_f^\pi$	R_{DCO}	A_P	Multipolarity
443	$4^+ \rightarrow 2^+$	1.23(13)	)^a	)^b
448	$6^+ \rightarrow 4^+$	)^a	)^a	)^b
465	$8^+ \rightarrow 6^+$	1.23911)	0.08(7)	E2
766	$2^+ \rightarrow 2^+$	)^a	)^a	)^b
795	$4^+ \rightarrow 4^+$	0.62(13)	-0.09(10)	M1/E2
771	$6^+ \rightarrow 6^+$	)^a	)^a	)^b
1110	$2^+ \rightarrow 0^+$	)^a	)^a	)^b
1207	$4^+ \rightarrow 2^+$	)^a	)^a	)^b
1242	$6^+ \rightarrow 4^+$	)^a	)^a	)^b
1234	$8^+ \rightarrow 6^+$	)^a	)^a	)^b

)^a insufficient statistics to measure gamma-ray intensity.

)^b Multipolarity could not be determined

58

Table 4.10: *Gamma-ray energies, R_{DCO} ratios (gated on $\Delta I = 2$ transitions), and polarization anisotropy (A_P) and the multipolarity assigned to gamma transitions in the ^{152}Gd decay scheme.*

Band 11:

$E_\gamma(keV)$	$I_i^\pi \rightarrow I_f^\pi$	R_{DCO}	A_P	Multipolarity
428	$5^+ \rightarrow 3^+$	1.11(16)	0.05(9)	E2
441	$7^+ \rightarrow 5^+$	1.29(14)	0.11(9)	E2
477	$9^+ \rightarrow 7^+$	)^a	0.12(9)	)^b
519	$11^+ \rightarrow 9^+$	)^a	)^a	)^b
535	$13^+ \rightarrow 11^+$	)^a	)^a	)^b
504	$3^+ \rightarrow 2^+$	)^a	)^a	)^b
1107	$5^+ \rightarrow 4^+$	)^a	)^a	)^b
1091	$3^+ \rightarrow 2^+$	)^a	)^a	)^b
679	$3^+ \rightarrow 4^+$	0.79(10)	-0.02(11)	M1/E2
634	$5^+ \rightarrow 6^+$	0.55(11)	-0.09(5)	M1/E2
1075	$7^+ \rightarrow 6^+$	)^a	-0.02(5)	)^b
1026	$9^+ \rightarrow 8^+$	)^a	)^a	)^b
996	$11^+ \rightarrow 10^+$	)^a	)^a	)^b
942	$13^+ \rightarrow 12^+$	)^a	)^a	)^b

)^a insufficient statistics to measure gamma-ray intensity.

)^b multipolarity could not be determined

CHAPTER 5   DISCUSSION

5.1 Spin and parity assignment

Band 1 through Band 7 were previously seen by [Cam07], in most cases to higher spin than in present work. This is because [Cam07] used a heavier ^{36}S beam as opposed to our ^{4}He beam, and delivered more angular momentum to the system. In the case of known γ-ray transitions, my task was to check the multipolarity assignment of γ-rays. Three new bands (9, 10, and 11) were seen in this data. In addition, several new linking transitions between these new bands and previously known structures were seen. My task here was to assign spin and parity to new levels where possible.

5.1.1 The ground state yrast band (Band 1)

The present data set only allowed spins $I \leq 18$ to be observed. For all transitions in Band 1, $R_{DCO} \sim 1$ and $A_P > 0$ are consistent with stretched E2 character.

5.1.2 Band 2

Previous work [Cam07, Wan05, and Zol80] has established Band 2 as a positive parity structure. [Wan05, Zol80] observed the bandhead to have a spin-parity of 0^+ and an excitation energy of 615.4keV. The structure of this band is confirmed by the level scheme constructed from our data set. Our data also reveal four (361keV, 259keV, 198keV and 159keV) new decays out of Band 2 to the negative parity Band 3, and one at 931keV connecting the 2^+ level of Band 2 to the 0^+ level of Band 1.

The first of these new linking transitions is a 361keV γ-ray connecting the 10^+ state of Band 2 to the 9^- state of Band 3. The DCO ratio (1.09(6)) gated on a dipole is consistent with that expected of a $\Delta I = 1$ transition. Although the A_p value (+0.01(2)) does not strongly suggest either magnetic or electric character, the 361keV γ-ray can be assigned E1 character since it connects previously known states of opposite parity, and must therefore have odd parity itself. The second linking transition (259keV, $8^+ \rightarrow 7^-$), and third linking transition (198keV, $6^+ \rightarrow 5^-$), are assigned E1 character based on similar arguments, even though in the case of the 198keV transition the DCO ratio (0.80(6)) is slightly lower than expected when gated on a dipole. Thirdly the 159keV ($4^+ \rightarrow 3^-$) decay is also assigned E1 character even though it was too weak to allow explicit measurement of the DCO ratio or polarization anisotropy. The 159keV transition is assigned E1 character because it connects two states of known opposite parity, and whose spins differ by one unit. The fourth linking transition is a 931keV γ-ray connecting the 2^+ state of Band 2 to the 0^+ state of the ground state yrast band. The DCO ratio of this transition (931keV) could not be determined. Its A_p value was found to be (+0.15(6)), which is consistent with stretched E2 character. Therefore we suggest an assignment of stretched E2 character to this transition.

5.1.3 Band 3

Band 3 had been established as a negative parity structure previously by [Cam07, Wan05, and Zol80]. The present data set only allowed spins $I \leq 21^-$ to be observed. A new transition (364keV) was observed decaying from the 3^- level feeding the 4^+ level in the ground state band. However, this gamma-ray is weak and there were not enough statistics to determine the DCO ratio and polarization anisotropy. Hence the multipolarity could not be determined experimentally. However, since the parities of the 3^- and 4^+ states were previously known, the transition is assigned E1 character. For the in-band transitions in Band 3, $R_{DCO} \sim 1$ and $A_P > 0$ are consistent with stretched E2 character for those measured. For the out of band transitions, $R_{DCO} \sim 0.73$ and $A_P > 0$ are consistent with stretched E1 character.

5.1.4 Band 4

[Cam07] observed this band up to I = 40 and suggested that it has negative parity and the band head at 2536.9keV has spin and parity of 8^-. There is a disagreement about the spin and parity of Band 4. Levels at 2537keV, 2890keV and 3346keV were observed both by [Wan05 and Zol80] who tentatively assigned spins of (9^+), (11^+) and (13^+). These levels are connected by 354keV $(10^- \rightarrow 8^-)$ and 457keV $(12^- \rightarrow 10^-)$ in-band E2 transitions. Band 4 is connected to the ground state yrast positive band by several transitions. Many were too weak to determine the DCO and A_p. However, the DCO and A_p values for two of the transitions support the assignment of unstretched, $\Delta I = 0$ E1 character. The two transitions are 591keV $(10^- \rightarrow 10^+)$ and 791keV $(8^- \rightarrow 8^+)$. This supports the spin and parity assignment of [Cam07] for this band. It is thus likely that, for example, the level at 2537keV has $I^\pi = 8^-$ and not 9^+ as assigned by [Wan05 and Zol80].

A new level $((6^-))$ below the 8^- level has been observed. This new level decays to the 6^+ level of Band 1 via a new transition which is the 947keV transition. The DCO and A_p values for the 947keV could not be determined due to poor statistics. Another new transition is the 364keV transition. It connects the new level with the 8^- level. The DCO ratio of the 364keV gamma-ray was measured to be 1.18(5) while gating on a quadrupole transition. This suggests that it is of quadrupole in nature. However, there were insufficient statistics to determine the polarization anisotropy of this gamma-ray. We therefore suggest a spin of 6 with negative parity tentatively assigned to the new level. For all in-band transitions in Band 4 where R_{DCO} and A_p could be measured, $R_{DCO}{\sim}1$ and $A_P{>}0$ are consistent with stretched E2 character.

5.1.5 Bands 5 and 6

These two bands are signature partners, and are therefore treated together. These two bands are typical of high-K structure joined by low energy M1 transitions. The spin and parity of Band 5 was established by [Cam07] down to 10^-, but the spin of the level below 10^- was uncertain. It was difficult to assign spin of the lowest level in Band 5. The DCO ratio and polarization anisotropy for the 284keV ($10^- \rightarrow (8)^-$) could not be determined. Some weaker decays from the lower levels are also observed in this band. In particular, the 827keV and 996keV γ-rays from the 10^- and $(8)^-$ levels respectively in Band 5. However, the DCO ratio and the polarization anisotropy for the 996keV ($(8^-) \rightarrow 7^-$) were found to be 0.63(6) and −0.057(4) respectively. Its DCO ratio was obtained by setting a gate on a $I \rightarrow I-1$ transition. This DCO ratio is not consistent with that expected of a pure dipole transition. Fig. 4.13 does not allow a firm conclusion. Fig. 4.13 is a plot of linear polarization P (θ) as a function of the mixing ratio for mixed M1/E2 transitions. These measurements of DCO and A_p make it hard to reach a firm conclusion about the character of the 996keV transition. However, calculations of DCO values as a function of δ for $I \rightarrow I-1 \rightarrow I-2$ transitions can help us to reach a conclusion about the character of this transition. Such a calculation is shown in Fig. 5.1. The DCO ratio obtained for the 996KeV is consistent with that of a mixed M1/E2 transition and its mixing ratio lies where the probability of an M1/E2 transition is ~50% as shown in Fig. 5.1.

The polarization anisotropy of the 996KeV transition was deduced from the sum of the 654KeV transition in Band 2 and the 284KeV transition in Band 5 gates. This was done because the intensities of this peak were somehow different from the different projections of the matrix. The polarization sensitivity Q for the 996KeV was found to be 0.17 using a graph of Q versus the energy of gamma rays [Jon95]. The relation between the polarization sensitivity Q and the polarization anisotropy is that given by equation 2.17.
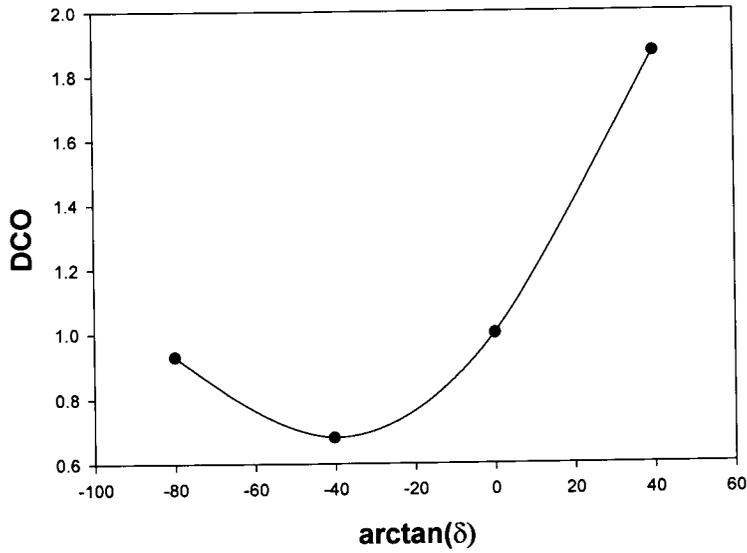
Figure 5.1: *A plot showing calculated DCO values as a function of the mixing ratio δ.*

Therefore the spin of the level below the 10^- level in Band 5 is tentative. [Cam07] also placed the 147keV ($10^- \rightarrow 9^-$) tentatively in Band 5. The DCO ratio of the 147keV was found to be 0.93(6) while gating on a $\Delta I = 1$ transition. This suggests that it is of $\Delta I = 1$ character. Its A_p value could not be determined. Signature partner bands in this mass region are typically connected by M1/E2 transitions. Therefore the 147keV transition is probably mixed M1/E2.

We observed several new transitions that connect Band 6 with other bands. One of the transitions is the 845keV γ-ray that connects the 13^- level in Band 6 with the 12^+ level of Band 1. Its DCO ratio (0.79(13)) gated on dipole is consistent with that expected of a $\Delta I = 1$ transition. Its A_p value was found to be (0.07(9)). This suggests that the 845keV γ-ray is an electric transition. Therefore the 845keV transition is assigned E1 character. We had insufficient statistics to determine the DCO ratio and polarization values for the other new transitions (680keV and 1132keV). Fig. 5.2 shows a plot of excitation energy as a function of spin for Bands 5 and 6. This plot suggests that these two bands are probably signature partners and are strongly coupled since there is only a small energy splitting.
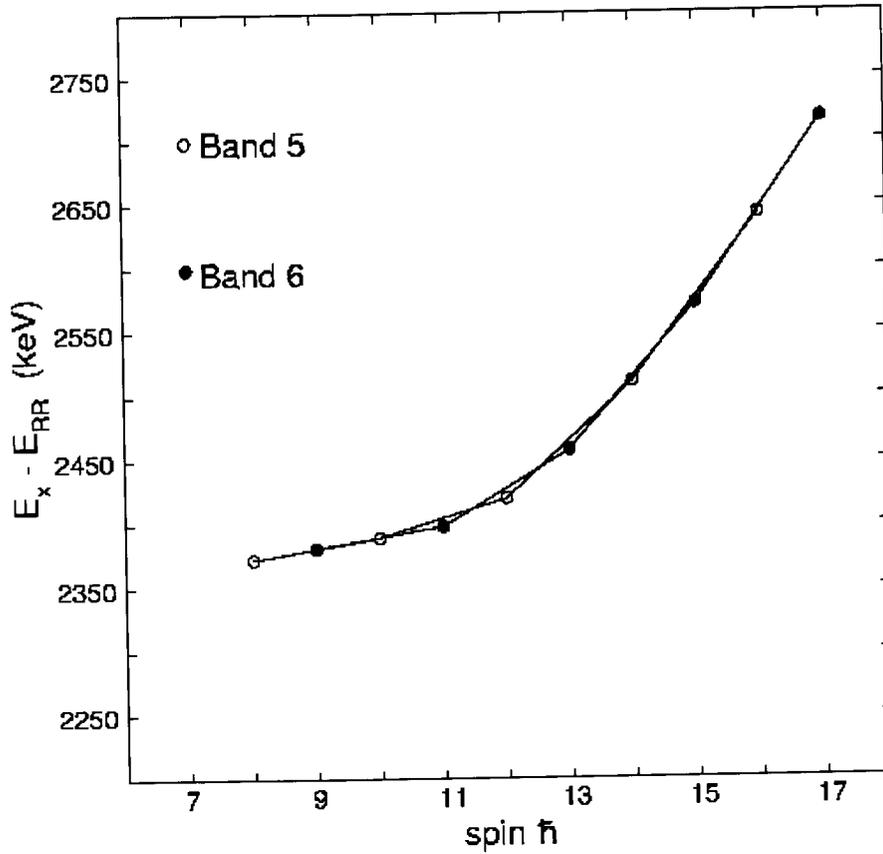
Figure 5.2: The rigid rotor plot of Bands 5 and 6 using $E_{RR} = E_{ex} - 7.0 * I(I+1)$.

5.1.6 Band 7

The present data set did not allow us to observe any new levels or transitions in this band. This band was previously established as a positive parity structure by [Cam07]. For all transitions in Band 7 where R_{DCO} and A_p could be measured, $R_{DCO} \sim 1$ and $A_P > 0$ are consistent with stretched E2 character.

5.1.7 Band 9

The energy levels obtained in this band are all new. The in-band transitions were too weak to measure DCO ratio and polarization anisotropy. Band 9 decays to the ground state band via the 704keV transition. The polarization anisotropy for the 704keV transition was found to be 0.19(5). This suggests that it is probably a stretched transition, but its DCO ratio could not be determined. Spin 14 in the level connecting Band 9 to the ground state band via the 704keV transition will be an impossible assignment as this will mean that the 704keV transition is an E3. Our data does not allow us to determine spin and parity of this band.

5.1.8 Band 10

This band has only three (443keV, 448keV and 465keV) in-band transitions. For the 441keV transition, the DCO ratio was found to be 1.23(13) while gating on the 448keV transition. This suggests that the 443keV and 448keV transitions are likely of the same multipolarity. However, the polarization anisotropy of this transition could not be determined due to poor statistics. The second transition is the 465keV. Its DCO ratio (1.23(11)) gated on the summed spectra (sum of 443keV and 448keV gates). This suggests that these transitions are likely of the same multipolarity. Its A_p value +0.08(7) does not strongly suggest electric or magnetic character. Band 10 is linked to the ground state band via several transitions. One of them is the 795keV transition which decays to the 4^+ level in Band 1. Its DCO ratio (0.62(13)) gated on the 448keV transition is consistent with that expected of a $\Delta I = 0$ mixed transition. Its polarization anisotropy was found to be -0.09(10), and it does not allow electric or magnetic assignment. Further, the rigid rotor plot in Fig. 5.3 shows that Band 10 is a rotational band. Therefore the three in-band transitions are likely to be of E2 character. The DCO ratio (0.62(13)) of the 795keV is consistent with that expected of a $\Delta I = 0$ mixed. Therefore 795keV is likely of M1/E2 character. Therefore Band 10 is likely a positive parity band and the level connected via the 795keV transition with the 4^+ level in Band 1 probably has spin and parity of 4^+.
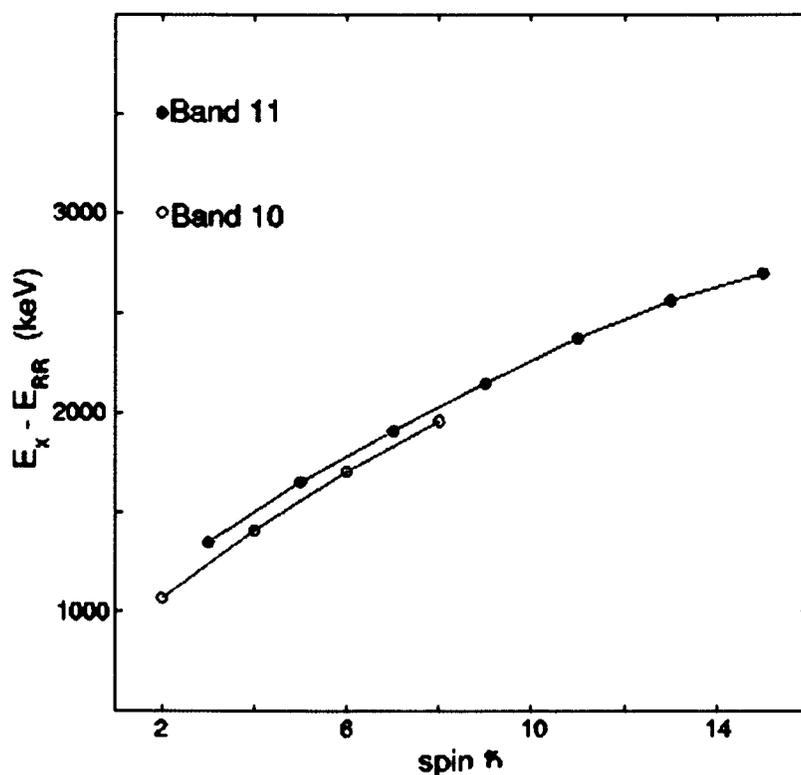
Figure 5.3: *The rigid rotor plot for Bands 10 and 11 using* $E_{RR} = E_{ex} - 7.0 * I(I+1)$.

5.1.9 Band 11

Previous studies by [Cam07, Wan05 and Zol80] did not observe transitions in this band. The rigid rotor plot shown in Fig. 5.3 suggests that Band 11 may be a rotational structure of E2 transitions. Our data allowed us to measure DCO ratios and A_p values for the two (428keV and 441keV) transitions from the first two levels in this band. The DCO ratio of the 428keV gated on the 441keV was found to be 1.11(16). This suggests that the two transitions are likely of the same multipolarity. Its A_p value was found to be +0.05(9), which suggests electric transition. We therefore suggest that the 428keV transition is of stretched E2 character. The DCO ratio (1.29(14)) of the 441keV transition gated on the 477keV transition suggest that the 441keV and 477keV transitions are likely of the same multipolarity. Its A_p value

(+0.11(10)) suggests that it is electric in nature. Therefore, the 441keV transition is assigned stretched E2. The other in-band transition is the 477keV. Its DCO ratio could not be determined, but its A_p value was found to be +0.12(10). This suggests that the 477keV transition is likely electric.

Band 11 is linked to energy levels in Band 2 via the 504keV transition which decays to the 2^+ level. However, due to insufficient statistics the DCO ratio and polarization anisotropy for this transition could not be measured. Several transitions link the ground state band with this band. However, there were not sufficient statistics to measure the DCO ratio and polarization anisotropy of some of these linking transitions. One of the linking transitions is the 634keV transition which decays to the 6^+ level in Band 1. Its DCO ratio (0.55(11)) gated on a quadrupole transition is consistent with that expected of a $\Delta I = 1$ transition. Its A_p value was found to be -0.09(5). Therefore the 634keV γ-ray is assigned M1/E2 character. The other linking transition was the 679keV transition, which decays to the 4^+ level of Band 1. Its DCO ratio (0.79(10)) gated on quadrupole transition is consistent with that of a $\Delta I = 1$ transition. Its A_p value was found to be -0.02(11), and it does not confirm electric or magnetic nature. The 679keV γ-ray can also be assigned M1/E2 character since the lowest level has been assigned spin and parity of 3^+. We also obtained the polarization anisotropy for the 1075keV transition linking to the ground state band through the 6^+ level to be -0.03(5). The DCO ratio of the 1075keV could not be determined. We therefore suggest that Band 11 is likely a positive parity band.

5.1.10 The states not assigned to bands (Unknown)

These states were included for completeness. The intensity of these states was very low. DCO ratios and polarization anisotropies could not be measured. Therefore our data did not allow us to assign any structure to these states since they do not exhibit $I(I+1)$ pattern.

5.2 Interpretation of bands

Band 1 is the ground state band of the nucleus ^{152}Gd. In the ground state the $\pi d_{5/2}$ [411] $3/2^+$ and $\nu i_{13/2}$ [660] $1/2^+$ orbitals correspond to the neutron and proton Fermi levels respectively. Band 1 is yrast up to spin $16\hbar$. The ground state quadrupole deformation of ^{152}Gd ($\beta_2 \sim 0.205$) is predicted to be very similar to that of the isotone ^{154}Dy ($\beta_2 \sim 0.198$) in calculations done by [Naz90]. Locally, in most isotonic chains the quadrupole deformation β_2 increases as the neutron number increases. For example, the β_2 values for other N = 88 isotones except for ^{150}Sm ($\beta_2 \sim 0.198$) are markedly different: ^{156}Er ($\beta_2 \sim 0.182$), ^{158}Yb ($\beta_2 \sim 0.167$), and ^{160}Hf ($\beta_2 \sim 0.141$). The same situation was observed by [Bro02] in the N = 89 isotones ^{153}Gd and ^{155}Dy.

Most deformed nuclei in the N = 90 range have bands based on the low-lying first excited $K^\pi = 0^+$ state. This band has usually been interpreted as a β-vibrational band [Bès63]. Band 2 is such a band in ^{152}Gd and it becomes yrast at $18\hbar$. The assignment of β-vibrational band to the lowest excited $K^\pi = 0^+$ state has been questioned by previous studies done by [Chas79 and She80]. It was recently suggested by [Sha06] that the $K^\pi = 0^+$ structure of Band 2 may not be a β-vibrational band. For example, calculations of the inverse moment of inertia parameter $(\hbar^2/2\Im)$ done by [She80] for the $K^\pi = 0^+$ (ground state and excited state) and the $K^\pi = 0^-$ bands suggested that the excited $K^\pi = 0^+$ and $K = 0^-$ bands are structurally more related to each other than to the ground state. Further, it was found out that the inverse moments of inertia for the excited $K^\pi = 0^+$ and $K^\pi = 0^-$ bands were similar, and there was a considerable difference from the value of the $\hbar^2/2\Im$ for the ground state $K^\pi = 0^+$ band. The separation of energy levels in Band 2 is very similar to that of the opposite parity and opposite signature octupole Band 3. This also suggests that they could be bands based on a static octupole deformation [Sha06].

The structure of the $K^\pi = 0^-$ states has been studied by [She80] who suggested three shape possibilities. In the first, [She80] suggested that the $K^\pi = 0^-$ states with $I^\pi = 1^-, 3^-$, 5^-, ... arise from an octupole vibration built on the ground state. In the second one

they superimposed a quadrupole deformation and a stable octupole deformation with a potential barrier between one octupole minimum and its mirror image. This gave rise to an alternating parity band, $I^\pi = 0^+, 1^-, 2^+, 3^-$ ...The mirror shapes gave two sets of levels, $I^\pi = 0^+, 2^+, 4^+,$ .....and $I^\pi = 1^-, 3^-, 5^-,$ ...with odd spins moved upward in energy compared to the even spins. The third possibility involved a coexistence of two shape minima, one near spherical or prolate reflection symmetric and static octupole band. They observed that the positive parity states in the octupole band mix with the ground state band and be pushed up in energy. Band 3 has been reported to be built on an octupole vibration by [Cam07, Wan05, and Zol80].

[Cam07] saw all negative parity structures up to band termination. Band termination phenomenon occurs when the Coriolis term aligns the angular momenta of individual single particles in a deformed rotating nucleus in the direction of the rotation axis. This rotational alignment of the individual particles creates a density distribution that is symmetric about the rotation axis. Band termination occurs when the density distribution about the rotation axis becomes symmetric, with the angular momentum being the sum of the contributions of aligned individual particles.

A similarity between ^{152}Gd and the isotone ^{154}Dy is also seen in the negative parity Bands 3 and 4. A plot of excitation energy minus the rotating liquid drop energy as a function of spin (Fig. 5.3) done by [Cam07] shows that at low-spin states, Bands 3 and 4 in ^{152}Gd show a change in curvature above $I = 20\hbar$ compared with the $(-, 0)_1$ and $(-, 0)_1$ bands in ^{154}Dy. This observation indicates a similar band crossing. Band crossing occurs when an excited band has a higher moment of inertia than the ground state band. What happens is that the energies of levels in the excited band will increase with increasing spin, and at high spin they can occur lower in energy than levels of the same spin of the ground state band. The notation $(-, 0)_1$ denotes (π, α), where π is the parity and α is the signature.

Band 4 was initially established by [Wan05 and Zol80] and they assigned odd spins with positive parity. As [Cam07] pointed out, Band 4 has an analogue in ^{154}Dy which is Band (-, 0)1. These bands show similar behaviour on the plot of excitation energy minus the rotating liquid drop against spin. That is clearly seen in Fig. 5.4. Thus [Cam07] assigned even spins and negative parity to Band 4. Our results are in agreement with the spin and parity assigned by [Cam07].
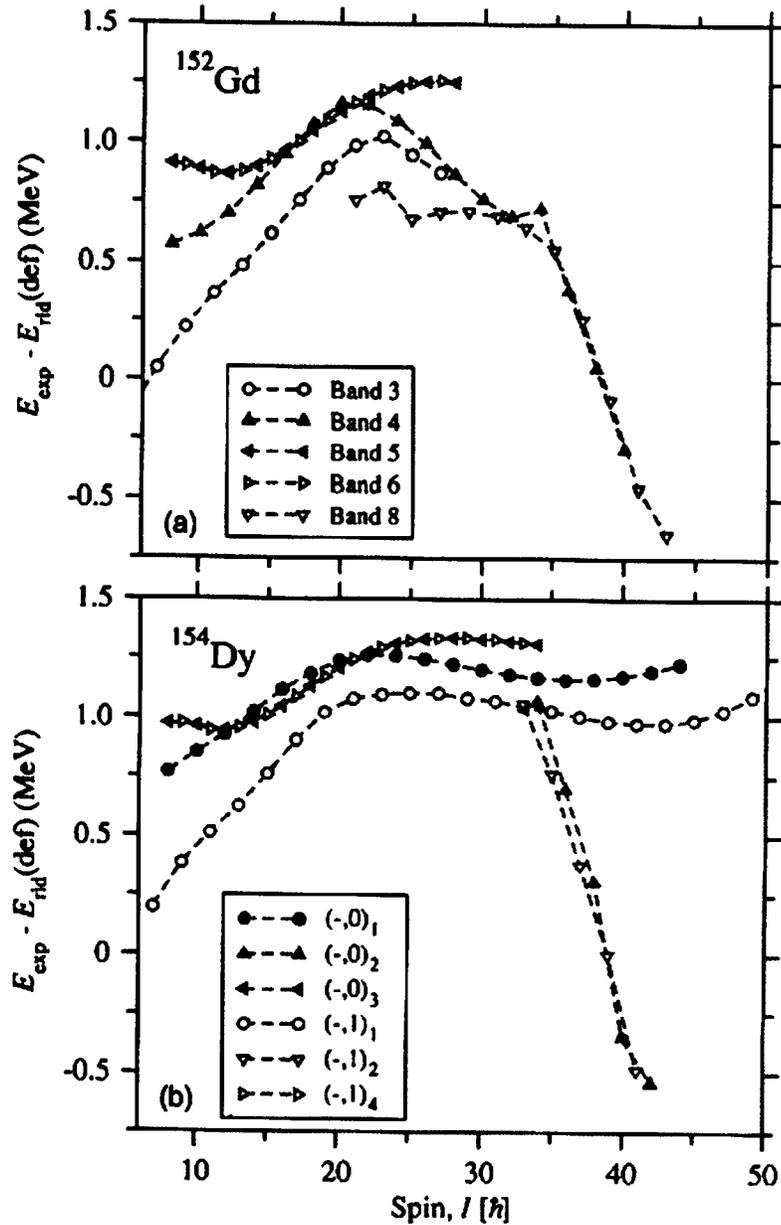

Figure 5.4: *Excitation energy minus the rotating liquid drop energy as a function of spin for the negative parity bands in ^{152}Gd and ^{154}Dy [Cam07].*

Bands 5 and 6 are likely the two signature partners of a strongly coupled band in the nucleus ^{152}Gd. Bands 5 and 6 show almost identical behavior to the signature pair (-, 0)$_3$ and (-, 1)$_4$ in ^{154}Dy in a plot of excitation energy minus the rotating liquid drop energy as a function of spin. This can be seen in Fig. 5.4. Measurements of B (M1)/B (E2) branching ratios for bands 5 and 6 done by [Cam07] in ^{152}Gd overlap within uncertainties of the (-, 0)$_3$ and (-, 1)$_4$ bands in ^{154}Dy. It was therefore concluded [Cam07] that this corresponding bands in ^{152}Gd and ^{154}Dy have the same configuration, ν [(i$_{13/2}$)^1 $\otimes$ (h$_{11/2}$)$^{-1}$] and very similar deformations.

Band 7 becomes yrast at 18$\hbar$. It was suggested by [Cam07] using Fig. 5.5 that Band 7 can be identified with the (+, 0)$_1$, (+, 0)$_2$, and (+, 0)$_3$ structures in ^{154}Dy. It was also observed that the (+, 0)$_1$ band in ^{154}Dy shows a rotational nature even in high spins, but that was not observed for the corresponding structure in ^{152}Gd after a spin of 28$\hbar$. The plot also showed that the portion I $\geq$ 28$\hbar$ of Band 7 is seen as a continuation of Band 1.
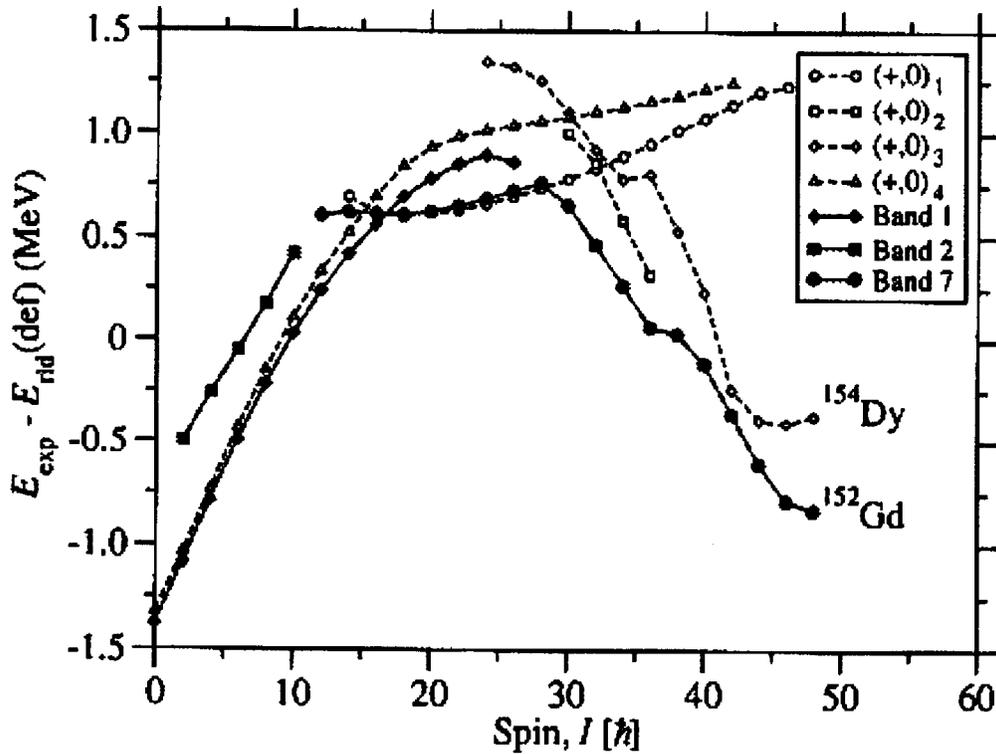
Figure 5.5: *Excitation energy minus the rotating liquid drop energy as a function of spin for high-spin positive–parity states in ^{152}Gd compared with the three lower energy states in ^{154}Dy, [Cam07].*

The positive parity Bands 10 and 11 have been suggested to be γ-vibrational bands based on the 2^+ level at 931keV by [Sha06]. A γ vibration is a K = 2 mode, and it is easy to distinguish it from a β band as it starts with 2^+ and contains the odd angular momenta as well. These bands were not observed in the previous studies done by [Cam07, Wan02, and Zol80]. We therefore do not have enough information on the behavior of Bands 10 and 11. Therefore future experiments should also be aimed at studying their behavior. The behavior of the rotational bands, terminating structures, negative-parity levels and positive-parity levels of the isotone ^{154}Dy are well explained in [Ma02].

CHAPTER 6   CONCLUSIONS

High spin states in ^{152}Gd have been studied via the ^{152}Sm (^{4}He, 4n) ^{152}Gd fusion evaporation reaction at a beam energy of 45MeV using AFRODITE array. Our (α, 4n) reaction successfully populated states well above the yrast line. We observed new structures in ^{152}Gd, and extended the previously known decay scheme.

The ground state band behaves normally since it shows the AB crossing phenomena. The negative parity bands all have a common bandcrossing demonstrated by a change in curvature when the excitation energy minus the rotating liquid drop energy is plotted against the spin. The nucleus ^{152}Gd shows very similar behavior with its isotone ^{154}Dy, and this supports angular momentum induced shape change in ^{152}Gd from prolate collective rotation toward oblate non-collective via band termination mechanism above spin 30ħ as reported by [Cam07].

New E1 decays from Band 2 to the octupole Band 3 have been observed. The DCO and linear polarization techniques used allowed us to assign multipolarity to these new E1 decays. The controversy that the low-lying first excited $K^\pi = 0^+$ state may not be a β band brings interesting physics in the structure and the behavior of the low-lying first excited $K^\pi = 0^+$ states in nuclei. We intend calculating the branching ratios $\dfrac{B(E_1)}{B(E_2)}$ for the new E1 transitions in Band 2 so that we can reach a conclusion about the $K^\pi = 0^+$ state in Band 2. Several new linking transitions have been observed in different bands. We had very poor statistics in the case of some gamma transitions and this brought some difficulties in measuring DCO ratios and linear polarization anisotropy of some new transitions. This also gave us problems in finding structures of new states observed and bands. However we were able to assign spin and parity of some levels in the weak Bands 10 and 11. We therefore conclude that the DCO and linear polarization techniques used are a fruitful tool to be used in the spin and parity measurements in states of deformed nuclei.

We intend to extend our measurements of the nucleus ^{152}Gd via ^{150}Sm (α, 2n) ^{152}Gd fusion-evaporation reaction. We have learnt that the (α, 4n) reaction used in the present analysis is contaminated by strong γ-rays from the (α, 3n) reaction to ^{153}Gd. We hope to resolve some uncertainties arising with new levels proposed from the (α, 4n) data using the (α, 2n) reaction. We also intend to study a different nucleus ^{150}Sm, via the ^{148}Nd (α, 2n) ^{150}Sm reaction. Little is known about (^{150}Sm). The nucleus ^{150}Sm has 88 neutrons and is known to have a fixed octupole deformation at higher spins, and this will also help us to understand aspects of the rotational evolutions of ^{152}Gd. Measurements on this nucleus will also help to balance recent measurements done by [Kul08] where they observed coexisting (nearly) identical bands in ^{152}Sm.

REFERENCE

[Bar08]   R.A. Bark, Summer School Lecture on Nucl. Phys. Mpumalanga-Skukuza, South Africa, 27 January-3 February (2008).

[Bès63]   D.R. Bès, Nucl. Phys. **49**, 544(1963).

[Bow71]   W.W. Bowman, T.T Sugihara, and F.R. Hamiter, Phys. Rev. **C 3**, 1275 (1971).

[Bro02]   T.B. Brown, M.A. Riley, D. Campbell, D.J. Hartley, F.G. Kondev, J. Pfohl, R.V.F. Janssens, S.M. Fischer, D. Nisius, P. Fallon, W.C. Ma, J. Simpson and J.F. Sharpey-Schafer, Phys. Rev. **C66**, 064320 (2002).

[But73]   P.A. Butler, P.E. Carr, L.L.Gadeken, A.N. James, P.J. Nolan, J.F. Sharpey-Schafer, P.J. Twin and D.A. Viggars, Nucl. Instr. and Meth. **108**, 497 (1973).

[Cam04]   D.B. Campbell, Ph.D Thesis, Florida State University, (2004).

[Cam07]   D.B. Campbell, R.W. Laird, M.A. Riley, J. Simpson, F.G. Kondev, D.J. Hartley, R.V.F. Janssens, T.B. Brown, M.P. Carpenter, P. Fallon, S.M. Fischer, T. Lauritsen, D. Nisius, and I. Ragnarsson, Phys. Rev. **C75**, 064314 (2007).

[Cas02]   R.F. Casten, Nuclear Structure from a Simple perspective, Second Edition, Oxford University Press Inc. New York, pg. 204 (2002).

[Cha79]   R.R. Chasman, Phys. Rev. **C42**, 630 (1979).

[Duc99]   G. Duchêne, F.A. Beck, P.J. Twin, G. de France, D. Curien, L. Han, C.W. Beausang, M.A. Bentley, P.J. Nolan and J. Simpson, Nucl. Instr. And Meth. **A 432**, 90 (1999).

[Gar86]   J.D. Garrett, Shape and Pair Correlations in Rotating Nuclei, The Niels Bohr Institute, University of Copenhagen, Lectures presented at the International School of Heavy ion Physics; Second Course, Erice, Italy, October 12-22, pg.7 and pg. 32 (1986).

[Gre96]   W. Greiner and J.A. Maruhn, Nuclear Models, Springer-Verlag Berlin Heidelberg, pg.158 (1996).

[Jon95]   P.M Jones, Nucl. Instr. and Meth. **A362**, 556 (1995).

[Kno79]   G.F Knoll, Radiation Detection and Measurement, John Wiley & Sons, pg. 643 (1979).

[Kra73]   K.S. Krane, R.M. Steffen and R.M. Wheeler, Nuclear Data Tables, **11**, 351(1973).

[Kra88]   K.S. Krane, Introductory Nuclear Physics, John Wiley & Sons,   pg. 198 and pg.335 (1988).

[Kul08]   W.D. Kulp, J.L. Wood, P.E. Garrett, C.Y. Wu, D. Cline, J.M. Allmond, D. Bandyopadhyay, D. Dashdorj, S.N. Choudry, A.B. Hayes, H. Hua, M.G. Mynk, M.T. McEllistrem, C.J. McKay, J.N. Orce, R. Teng, and S.W. Yates, Phys. Rev. C77, 061301 (2008).

[Lee02]   J.H. Lee, C.S. Lee, J.Y. Moon, Y.K. Kwon, Y. Gono, T. Fukuchi, S. Tanaka, T. Shinozuka, M. Fujita, A. Yamazaki, T. Sonoda, Y.K. Kim and J.S. Chai, Jou. Of Korean Phys. Soc. **40**, 793 (2002).

[Leo87]   W. R. Leo, Technique for Nuclear and Particle Physics Experiment, Lausanne, pg. 113 (1987).

[Lie84]   R.M. Lieder, H. Jäger, A. Neskakis, T. Venkova and C. Michel, Nucl. Instr. and Meth. In Phys. Res. **220**, 363 (1984).

[Lil01]   J. Lilley, Nuclear Physics principles and Applications, John Wiley & Sons. Pg. 136 (2001).

[LØv72]   G. LØvhØiden, S.A. Hjorth, H. Ryde and L. Harms-Ringdahl, Nucl. Phys. **A 181**, 589(1972).

[Ma02]   W.C. Ma, R.V.F. Janssens, T.L. Khoo, I. Ragnarsson, M.A. Riley, M.P. Carpenter, J.R. Terry, J.P. Zhang, I. Ahmad, P. Bhattacharyya, P.J. Daly, S.M. Fischer, J.H. Hamilton, T. Lauritsen, D.T. Nisius, A.V. Ramayya, R.K. Vadapalli, P.G. Varmette, J.W.Watson, C.T. Zhang, and S.J. Zhu, Phys. Rev. **C65**, 034312 (2002).

[Mab03]   G.K. Mabala, PhD thesis, University of Cape Town, (2003). Unpublished.

[Mal06]   M.S. Maliage, MSc thesis, University of the Western Cape, (2006). Unpublished.

[Mar70]   P. Marmier and E. Sheldon, Physics of Nuclei and Particles, Vol. II, Academic Press, Inc. pg.1230 and pg. 1292 (1970).

[Mor74]   H. Morinanga and T.Yamazaki, In-Beam Gamma –Ray Spectroscopy, Elsevier North-Holland Inc. New York, pg. 50 (1974).

[Naz90]   W. Nazarewicz, M.A. Riley, and J.D. Garrett, Nucl. Phys. **A512**, 61 (1990).

[New98]   R.T. Newman, J.J. Lawrie, B.R. S. Babu, M.S. Fetea, S.V. Förtsch, S. Naguleswaran, J.V. Pilcher, D.A. Raavé, C. Rigollet, J.F. Sharpey-Schafer, C.J. Stevens, F.D. Smit, G.F. Steyn, C.V. Wikner, D.G. Aschman, R. Beetge, R.W. Fearick, G.K. Mabala, S. Murray, D.G. Roux, W. Whittaker and N.J. Ncapayi, proceedings of Balkan School on Nucl. Phys. September 1-10, Baltalimani, Istanbal-Turkey, Balkan Phys. Lett., 182 (1998).

[Rad95]   D.C. Radford, Nucl. Instr. And Meth. Phys. Rev. **A306**, 297 (1995).

[Rou01]   D.G Roux, PhD thesis, University of Cape Town, (2001).

[Sha06]   J.F. Sharpey-Schafer, S.M. Mullins, R.A. Bark, E. Gueorguieva, J. Kau, F. Komati, J.J. Lawrie, P. Maine, A. Minkova, S.H.T. Murray, N.J. Ncapayi, and P. Vymers, Proc. XLIV Int. Winter Meeting on Nucl. Phys., Bormio, Italy January 29-February 5, (2006).

[She80]   R.K. Sheline, Phys. Rev. **C21**, 1660(1980).

[Shi07]   O Shirinda, Msc thesis, University of the Western Cape, (2007).

[Tan97]   T. Tanaka, F. Sakata, T. marumori, and K. Lwasawa, Phys. Rev. **C 56**, 180 (1997).

[Twi73]   P.J. Twin, Nucl. Instr. and Meth. **106**, 481 (1973).

[Wan05]   S. Wang, H. Hua, J. Meng, Z.H. Li, S.Q. Zhang, F.R. Xu, H.L. Liu, Y.L. Ye, D.X. Jiang, T. Zheng, Q.J. Wang, Z.Q. Chen, C.E. Wu, G.L.

Zhang, D.Y. Pang, J. Wang, J.L. Lou, B.Guo, and G. Jin, Phys. Rev. **C72**, 024317 (2005).

[Zol80]   D.R. Zolnowski, M.B. Hughes, J. Hunt, and T.T. Sugihara, Phys. Rev. **C 21**, 2556 (1980).